広島大学学位請求論文

Study of tensor renormalization group algorithm toward application to field theory

(場の理論への応用へ向けたテンソル
くりこみ群アルゴリズムの研究)

２０１９年

広島大学大学院理学研究科
物理科学専攻

上野　崚一郎

主論文

Study of tensor renormalization group algorithm toward application to field theory

Ryoichiro Ueno

Department of Physics, Graduate School of Science,
Hiroshima University

Thesis, March 2019

Abstract

I review the tensor renormalization group (TRG) algorithm and propose a new algorithm to improve the accuracy of the truncation involved in TRG algorithm. TRG has been developed and investigated to study critical phenomena in nature in terms of statistical mechanics. Although the renormalization group (RG) theory has been widely applied to investigate critical phenomena, TRG brings new insight into RG so that a part of difficulties in RG theory, such as the block spin transformations can not be exactly constructed for general systems, is resolved. Especially TRG is free from the Monte Carlo simulations and is applicable to systems with complex numbered Hamilton. This means that TRG could be free from the so called sign problem. The lattice quantum chromodynamics (LQCD) at non-zero chemical potential has this sign problem so that the nature of high density matter of hadrons is not yet quantitatively understood from the first principle. If TRG is applicable to LQCD, TRG could be one of the resolution to investigate the nature of high density matter as it is free from the sign problem. Before applying TRG to LQCD, several difficulties remain to resolve in TRG. In this thesis I focus on the improvement on the truncation algorithm used in TRG. In TRG, the partition function represented in a tensor product form will be evaluated recursively by repeating a singular value decomposition and partial tensor contraction. To reduce the computational cost, the dimensionality of tensor is truncated at every singular value decomposition. This truncation is the key point of TRG to be effective, however, this introduces unwanted behavior, discontinuous jumps on observables, when the system parameter is varied with a fixed small truncation cutoff. The origin of the jump has not yet been understood well so far, I confirm that the level crossing of singular value at the truncation cutoff occurs when the system parameter cross the jump. In this thesis I further uncover the origin of the jump in terms of the properties of the singular vectors associated with the singular values crossing the cutoff. Having been the nature of the jump, I propose a method to relax the irregular behavior in TRG by introducing a smooth cutoff in the truncation process. Two smooth cutoff procedures are introduced and investigated in the two dimensional Ising model and the effectiveness of the the proposed method is discussed.

Contents

1 Introduction

In the particle physics the theories for elementary interactions are explained by gauge theories. The theory of strong interaction, which explains the formation of atomic nuclei in terms of quarks and gluons, is the SU(3) non-Abelian gauge theory and the theory is called quantum chromodynamics (QCD). QCD has two interesting properties. One is the asymptotic freedom and another is the quark confinement. The asymptotic freedom is the property that the interaction strength logarithmically vanishing in the short distance due to the renormalization effect of the theory. This means that the coupling constant of the theory depends on the energy scale of the interaction where events take place. Quarks and gluons behave as free particles in high energy (short distance) scale. Thanks to this asymptotic freedom property, QCD can be systematically analyzed in terms of the coupling expansion using the standard perturbation theory. In contrast to the asymptotic freedom, the mechanism of the quark confinement is not theoretically established and it is only known that the qualitative behavior of the coupling constant in the long distance, where the interaction becomes strong. To understand the quark confinement, moreover, the formation of proton or neutron, a non-perturbative treatment of QCD is required. The lattice QCD (LQCD) has been invented by K. G. Wilson [1] to understand the confinement of quark non-perturbatively. The formulation is based on Feynman's path-integral formulation of quantum systems, however, LQCD regularizes the continuous and infinite space-time to a discretized finite sized lattice grid so that the path-integral is approximated to a multi-dimensional integration with finite degrees of freedom. On the lattice the gauge symmetry, which is the most important property of gauge theories, is maintained. With this lattice regularization, the numerical computation of LQCD became possible and has been successfully applied to study the properties of QCD.

One of the current concerns in LQCD is to determine the properties in finite temperature and density environments, such as the phase diagram or the equation of state of quark-gluon plasma phase. The finite temperature in zero baryon (quark) chemical potential (zero density) QCD has been studied using LQCD and the quark-gluon phase transition and the chiral phase transition have been quantitatively investigated. Improving the accuracy of the phase transition temperature

and the equation of state in zero density is being carried out using LQCD equipped with super-computers. On the other hand the properties in finite density are not yet precisely extracted from QCD and effective theories have been used. The main obstacle to the finite density calculation of LQCD is the existence of the so called sign problem in the simulation algorithm. The simulation algorithm used in LQCD is based on the Monte Carlo method by which the Feynman's path integral is evaluated numerically at a low computational cost. This requires that the weight function in the integrant should be real and non-negative. The action of LQCD in zero density satisfies this requirement. However introducing the baryon chemical potential in LQCD yields a complex phase to the action, which prevent us to utilize the Monte Carlo method. The appearance of complex numbers in the weight is generally called sign problem. Although several algorithms have been proposed to tackle the sign problem [2–18], no efficient algorithm to avoid the sign problem within simulation algorithms based on the Monte Carlo method.

The tensor renormalization group (TRG) method [19] is one of the promising method to avoid the sign problem. TRG was successfully applied to investigate the two dimensional Ising model in the pioneering work by Levin and Nave [19], where the critical point of the finite temperature phase transition was quite efficiently and accurately evaluated with TRG. After their work TRG has been realized to be a very effective method to investigate the phase transition phenomena in statistical physics. Many Intensive studies [20–32] have been carried out on the application of TRG to quantum field theories in recent years. Several difficulties are realized in applying TRG to practical quantum field theories such as Yang-Mills gauge theory in four-dimension. The major bottleneck of TRG to the practical lattice field theories is the exponential growth of the computational cost in the dimensionality of the system. TRG in [19] has been applied to the two-dimensional Ising model so that the cost is rather mild. A naive extension to the D dimensional Ising model shows that the cost becomes large.In order to keep the accuracy of TRG at low computational cost for a four dimensional lattice field theory, TRG still needs various improvements in the methodology. Several exploratory studies have been carried out to reduce the computational cost in higher dimensional models [33–35]. Other problem is that the numerical result from TRG has the irregular parameter dependence. In this thesis I focus on this irregular behavior and I propose an idea to suppress the behavior.

The structure of this thesis is as follows. In chapter 2 I give the brief review of QCD and LQCD. In section 2.1 I explain the property of the strong interaction, and the reason why LQCD is important. In section 2.2 I give Lagrangian for QCD. LQCD is explained in section 2.3. The path integral on which LQCD is based is

defined in subsection 2.3.1. The form of Lagrangian and the action for gluons and fermions in the lattice are discussed in subsections 2.3.2 and 2.3.3, respectively. In section 2.4 I explain the sign problem. TRG, which is used to avoid the sign problem, is introduced in chapter 3. As an example I apply TRG to the two dimensional Ising model in this thesis. The algorithm is given in section 3.1, and several results are shown in section 3.2. In chapter 4 I study about the irregular behavior of result from TRG. In section 4.1 I show the origin of the behavior and propose the idea to suppress it. The former and the latter are studied in subsection 4.1.1 and 4.1.2, respectively. I test the above idea and the numerical result is shown in section 4.2. Finally I summarize this thesis and express the outlook in chapter 5.

2 Lattice Gauge Theory

n the particle physics, all known elementary particles and interactions in nature are classified by the standard model. One of the notable structure of the standard model is that all elementary interactions named strong, weak, and electromagnetic, are uniquely determined by gauge principle. The standard model is a composition of three gauge theories. The nuclear force among protons and neutrons is very strong than the repulsive electric force among protons to form an atomic nuclei. The nuclear force now a days is not a fundamental interaction but a kind of covalent bonding emerging from exchanging virtual pions. More fundamentally protons, neutrons, and pions are all composite particles made of quarks and binded by a quark-quark interaction which is called strong interaction. The quark-quark interaction is mediated by gluons, which is very similar to that the electromagnetic interaction between electrons is mediated by photons. The dynamics of quarks and gluons are described by so called the quantum chromodynamics (QCD), which is one of the component of the standard model. Similar to the electromagnetic theory, which is based on the U(1) gauge symmetry, QCD is based on the SU(3) gauge symmetry. The properties of quarks and gluons, which are appeared as fundamental degrees of freedom in very high energetic collider experiments, are well described in terms of QCD. The success of QCD at the high energy experiments is due to the property of asymptotic freedom, the coupling constant is small in the high energy region, which enables us to utilize the standard perturbation theory. In the high energy scale quarks behave as free particles, which is called asymptotic freedom. On the other side, in the low energy scale the strength of interaction becomes strong so that the standard perturbation theory fails. The experiment fact that an isolated quark is not observed in nature is an important property of QCD. Theoretically all physical properties of hadrons, composite particles of quarks, should be explained in terms of QCD. However this is difficult technically due to strong interaction strength originating from the non-linear property of the interaction. In order to analyze QCD non perturbatively, K. G. Wilson invented Lattice QCD (LQCD) in 1974 [1] by reformulating SU(3) gauge theory on a lattice grid (discretized space-time). The discretized space-time has been introduced as the UV-cutoff which is inevitable to regularize any quantum field theory, the gauge symmetry was maintained exactly on the lattice by introduc-

ing gauge link variables as the element of SU(3) group. This construction enables us to define Feynman's path integral of QCD mathematically well defined and opens a way to numerical simulations without perturbation expansion in the coupling constant. LQCD is one of the most important tool to investigate the properties of quark sector from the first-principle in the standard model today.

In this chapter I briefly review the properties of strong interaction and the formulation of LQCD. The last section of this chapter is devoted to describe the sign problem of QCD which emerges in studying the properties of QCD with finite quark (baryon) chemical potential.

2.1 Strong Interaction

The strong interaction has two important properties; the quark confinement and the asymptotic freedom. The former says that we cannot observe an isolated quark, and the latter says that the coupling constant becomes weak in short distance. In this section I explain these properties using a phenomenological potential model between static quarks.

A static potential for a pair of quark and anti-quark separated by r is known phenomenologically as

$$V(r) \propto -\frac{g^2(r)}{r} + \sigma r + V_0, \tag{2.1}$$

where $g(r)$ is the effective coupling constant, and σ is a proportionality factor called the string tension. Using the potential (2.1), experimental results, e.g. mass spectrums of quarkonium, are explained. In (2.1), the Coulomb term dominates in small r region, but the linear term becomes dominant in large r. It means that we need infinite energy to observe an isolated quark, but it is impossible due to the pair production of quark and anti-quark. This phenomena in the long distance is called quark confinement, and it is caused by the linear term in eq. (2.1).

On the other hand, in the short distance the effective coupling constant $g(r)$ becomes zero asymptotically.This phenomena is called asymptotic freedom. As explained in the preamble of this chapter, the property of asymptotic freedom makes the perturbative QCD self consistent in sufficiently high energy region as the reliability of coupling expansion increases in weak coupling region. To study QCD in the low energy region, however, we need a new method other than the perturbation theory. LQCD is one of the non-perturbative theory by which we can study the physics of the strong interaction in the low energy region where the non-perturbative effect cannot be neglected.

2.2 QCD

Theory for the strong interaction is non-abelian SU(3) gauge theory. Quark and anti-quark fields is written as follows,

$$\psi(x) = \begin{pmatrix} \psi_1(x) \\ \psi_2(x) \\ \psi_3(x) \end{pmatrix}, \quad \overline{\psi}(x) = \begin{pmatrix} \overline{\psi}_1(x) & \overline{\psi}_2(x) & \overline{\psi}_3(x) \end{pmatrix}, \tag{2.2}$$

where subscripts 1, 2 and 3 indicate the degrees of freedom for the color charge. The components of $\psi_i(x)$ are Dirac fields, and anti-quark fields are defined as $\overline{\psi}_i(x) \equiv \psi_i^\dagger(x)\gamma_0$. Here γ_μ is Dirac gamma matrix. Gluon fields which are carriers of the strong interaction among quarks and anti-quarks are written as

$$A_\mu(x) = A_\mu^a(x)T_a, \qquad a = 1, \ldots, 8. \tag{2.3}$$

Here T_a is a generator of SU(3) group and I give the specific expressions in appendix A.

The Lagrangian for QCD is invariant under the SU(3) gauge transformation,

$$V(x) = \mathrm{e}^{g_0\theta^a(x)T_a}, \qquad i = 1, \ldots, 8, \tag{2.4}$$

where g_0 is a bare coupling constant and θ^a is a parameter of gauge transformation. Gauge transformations for quark and gluon fields are defined by

$$\psi'(x) = V(x)\psi(x), \quad \overline{\psi}'(x) = \overline{\psi}(x)V^\dagger(x), \tag{2.5}$$

$$A'_\mu(x) = V(x)A_\mu V^\dagger(x) + \frac{1}{g_0}V(x)\partial_\mu V^\dagger(x), \tag{2.6}$$

respectively. Using covariant derivative,

$$D_\mu \equiv \partial_\mu + g_0 A_\mu, \tag{2.7}$$

we obtain the Lagrangian for quark field which is invariant under the gauge transformations (2.5) and (2.6) as,

$$\mathscr{L}_\mathrm{q} = -\overline{\psi}(x)(\gamma^\mu D_\mu + m)\psi(x), \tag{2.8}$$

where m is the quark mass. The Lagrangian for the gluon field is also obtained as

$$\mathscr{L}_\mathrm{g} = -\frac{1}{2}\mathrm{Tr}[F_{\mu\nu}F^{\mu\nu}] = -\frac{1}{4}F^a_{\mu\nu}F^{a\mu\nu}, \tag{2.9}$$

where the field strength $F_{\mu\nu}$ is given by

$$F_{\mu\nu} = F^a_{\mu\nu}T_a \equiv \frac{1}{g}[D_\mu, D_\nu] = \partial_\mu A_\nu - \partial_\nu A_\mu + g_0[A_\mu, A_\nu]. \tag{2.10}$$

From eqs. (2.8) and (2.9) the Lagrangian for QCD is written by

$$\mathscr{L}_\mathrm{QCD} = \mathscr{L}_\mathrm{q} + \mathscr{L}_\mathrm{g}. \tag{2.11}$$

2.3 LQCD

In the previous section I showed the form of the Lagrangian for QCD (2.11). In this section I give the Lagrangian for LQCD and show several numerical results obtained using LQCD.

2.3.1 Path Integral

To define LQCD the path integral is usually used for the quantization. This formulation is proposed by R. P. Feynman in 1948 [36]. In this formulation the expectation value $\langle \mathcal{O} \rangle$ of an observable $\mathcal{O}$ is described as the summation over all possible paths between the initial and final state weighted by the action $S[\phi]$,

$$\langle \mathcal{O} \rangle = \frac{1}{Z} \int \mathcal{D}\phi \; \mathcal{O} \mathrm{e}^{\mathrm{i}S[\phi]}, \tag{2.12}$$

where the partition function Z is given by

$$Z = \int \mathcal{D}\phi \; \mathrm{e}^{\mathrm{i}S[\phi]}. \tag{2.13}$$

The measure of path integral $\mathcal{D}\phi$ is equivalent to the product of measures for all variables ϕ in the action $S[\phi]$. In LQCD approach, the path integral is redefined on the euclidian space-time finite lattice with momentum cut-off, and the non-pertuabative calculation is just available.

2.3.2 Gluons on the Lattice

The lattice field theory is defined on the euclidian four dimensional hyperspace whose volume is $V = L_1 \times L_2 \times L_3 \times T$,

$$\Gamma = \left\{ x \,\middle|\, x \in \mathbb{Z}^4, 0 \leq x_k \leq L_k, 0 \leq x_4 \leq T; k = 1, 2, 3 \right\}. \tag{2.14}$$

Linear size of each directions are arbitrary, but I take $L_k = T \equiv L$ unless otherwise noted in the following. In the lattice field theory the hyperspace (2.14) is descritized by introducing the lattice spacing a, and the fields are defined on the lattice. It means that coordinates x are replaced with sites n on the lattice,

$$x \to an = a(n_1, n_2, n_3, n_4), \qquad n_\mu = 0, 1, \ldots, L/a, \tag{2.15}$$

and quark fields $\psi(x)$ is defined on the site, $\psi(x) \to \psi(n)$. Gluon fields on the lattice, $U_\mu(n)$, correspond to the translation operator of quark field $\psi(n)$,

$$\psi_\parallel(n + \hat{\mu}) = U_\mu(n)\psi(n), \tag{2.16}$$

and $U_\mu(n)$ is called the link variable since it is defined on the link between sites on the lattice. $\hat{\mu}$ in eq. (2.16) is the unit vector in μ-th direction μ and its norm is $|\hat{\mu}| = 1$. The link variable $U_\mu(n)$ is written by the gauge field $A_\mu(n)$ as

$$U_\mu(n) = \mathrm{e}^{ag_0 A_\mu(n)}. \tag{2.17}$$

The gauge transformation of link variable is defined as follows,

$$U'_\mu(n) = V(n)U_\mu(n)V^\dagger(n+\hat{\mu}). \tag{2.18}$$

From eq. (2.18) a trace of link variables on a closed path C, $\mathrm{Tr}[\mathrm{P}[\prod_C U]]$, is gauge invariant, where P is the operator of the path ordered product. The Lagrangian of gluon on the lattice, which corresponds to the one in the continuum theory eq. (2.9), is written as

$$\mathscr{L}_{\mathrm{W}} = \frac{1}{g_0^2} \sum_{\substack{\mu,\nu \\ (\mu\neq\nu)}} \Re\left[\mathrm{Tr}\left[1 - P_{\mu\nu}(n)\right]\right], \tag{2.19}$$

where $P_{\mu\nu}(n)$, called plaquette, is defined by the products of link variables on the smallest square on the lattice,

$$P_{\mu\nu}(n) = U_\mu(n)U_\nu(n+\hat{\mu})U^\dagger_\mu(n+\hat{\nu})U^\dagger_\nu(n). \tag{2.20}$$

Therefore the action of gluon fields on the lattice is given by the summation of the Lagrangian (2.19) over the all lattice points,

$$S_{\mathrm{W}} = \frac{1}{g_0^2} \sum_n \sum_{\substack{\mu,\nu \\ (\mu\neq\nu)}} \Re\left[\mathrm{Tr}\left[1 - P_{\mu\nu}(n)\right]\right]. \tag{2.21}$$

The above action (2.21) is called the Wilson gauge action or the plaquette action [1]. Note that the form of the action on the lattice has an arbitrariness, because essentially important thing is that the action of LQCD in the continuum limit $a/L \to 0$ should be the original action defined from the Lagrangian of QCD (2.8) and (2.9).

2.3.3 Fermions on the Lattice

To obtain the action for quarks on the lattice, one should replace the covariant differential operator in (2.8) to the lattice covariant differential operator to maintain the lattice gauge symmetry. The lattice regularization to the fermion action introduces another kind of difficulty in the lattice theory. The massless fermion in the continuum space-time possesses chiral symmetry, which is the important property

when the low energy physics of QCD is discussed in terms of light mesons such as pion's and Kaon's. The important property of QCD in the low energy scale is the spontaneous symmetry breaking of the flavor chiral symmetry of $\mathrm{SU_L(3)xSU_R(3)}$ when up, down, and strange quarks are considered. The naive construction of lattice fermion action, unfortunately, yields an unwanted effect of the particle spectrum of the fermion action, so called species doubling problem, where 16 massless quarks are involved in the naive lattice action. This is known as the doubling problem. To avoid the problem one often adds an additional term called the Wilson term, and one obtain the action for quarks on the lattice as the following form [37],

$$S_{\mathrm{W}} = a^4 \sum_n \bar{\psi}(n) \left[\frac{1}{2} \sum_\mu \left\{ \gamma_\mu \left(\nabla^*_\mu + \nabla_\mu \right) - ar \nabla^*_\mu \nabla_\mu \right\} + m \right] \psi(n), \tag{2.22}$$

where $0 < r \leq 1$ is the Wilson parameter which is usually taken to be $r = 1$. The forward and the backward differences are defined as,

$$\nabla_\mu \psi(n) = \frac{1}{a} \left[U_\mu(n) \psi(n + \hat{\mu}) - \psi(n) \right] \tag{2.23}$$

$$\nabla^*_\mu \psi(n) = \frac{1}{a} \left[\psi(n) - U^\dagger_\mu(n - \hat{\mu}) \psi(n - \hat{\mu}) \right] \tag{2.24}$$

respectively. The action (2.22) is called the Wilson fermion action [1]. Note that the form of the action on the lattice has an arbitrariness as is the case in the action for gluons on the lattice.

In the Wilson fermion action (2.22) the Wilson term gives the discretization error of $O(a)$, while the Wilson gauge action has the error of $O(a^2)$. Practically controlling the error of $O(a)$ is hard, so the improvement procedure is studied [38–40]. To cancel the error of $O(a)$ B. Sheikholeslami and R. Wohlert proposed an additional term of the additional five dimensional operator [41],

$$S_{\mathrm{imp.}} = a^4 \ \frac{\mathrm{i}}{4} a \kappa r c_{\mathrm{SW}} \bar{\psi}(n) \sigma_{\mu\nu} \hat{F}_{\mu\nu}(n) \psi(n), \tag{2.25}$$

where $\sigma_{\mu\nu} = (\mathrm{i}/2)[\gamma_\mu, \gamma_\nu]$, κ is the hopping parameter,

$$\kappa = \frac{1}{2ma + 8r}, \tag{2.26}$$

$\hat{F}_{\mu\nu}(n)$ is the clover type field strength,

$$\hat{F}_{kl} = \frac{1}{8a^2} \left(Q_{\mu\nu}(n) - Q_{\nu\mu}(n) \right), \tag{2.27}$$

$$\begin{aligned} Q_{\mu\nu}(n) =& U_\mu(n) U_\nu(n + \hat{\mu}) U^\dagger_\mu(n + \hat{\nu}) U^\dagger_\nu(n) \\ &+ U_\nu(n) U^\dagger_\mu(n - \hat{\mu} + \hat{\nu}) U^\dagger_\nu(n - \hat{\mu}) U_\mu(n - \hat{\mu}) \\ &+ U^\dagger_\mu(n - \hat{\mu}) U^\dagger_\nu(n - \hat{\mu} - \hat{\nu}) U_\mu(n - \hat{\mu} - \hat{\nu}) U_\nu(n - \hat{\nu}) \\ &+ U^\dagger_\nu(n - \hat{\nu}) U_\mu(n - \hat{\nu}) U_\nu(n + \hat{\mu} - \hat{\nu}) U^\dagger_\mu(n), \end{aligned} \tag{2.28}$$

and $c_{\rm SW}$ is the coefficient known as the following [42],

$$c_{\rm SW} = \frac{1 - 0.656 g_0^2 - 0.152 g_0^4 - 0.054 g_0^6}{1 - 0.922 g_0^2}, \quad 0 \leq g_0 \leq 1. \tag{2.29}$$

The action for quarks on the lattice with the discretization error of $O(a^2)$ is written as

$$S_{\rm WC} = S_{\rm W} + S_{\rm imp.}, \tag{2.30}$$

and it is called the Wilson clover action or $O(a)$-improved Wilson fermion action.

Using actions (2.9) and (2.30), the vacuum expectation value of a correlation function for observables $O_1, O_2, \ldots, O_n$ is given by the following form,

$$\langle 0 \,|\, \mathrm{T}\,(O_1 O_2 \cdots O_n) \,|\, 0 \rangle = \frac{1}{Z_{\rm WC}} \int \mathcal{D}U \;\; \langle O_1 O_2 \cdots O_n \rangle_{\rm Wick} \det\left(D_{\rm WC}[U]\right) \mathrm{e}^{-S_{\rm W}}, \tag{2.31}$$

$$Z_{\rm WC} = \int \mathcal{D}U \;\; \det\left(D_{\rm WC}[U]\right) \mathrm{e}^{-S_{\rm W}} \tag{2.32}$$

where T is the operator of the time ordered product, and $D_{\rm WC}$ is the $O(a)$-improved Wilson Dirac operator defined as

$$S_{\rm WC} = a^4 \sum_{n,m} \bar{\psi}(n) D_{\rm WC}[U]_{(n,m)} \psi(m). \tag{2.33}$$

$\langle O_1 O_2 \cdots O_n \rangle_{\rm Wick}$ in eq. (2.31) means that all pairs of fermion and anti-ferion fields involved in the operators are replaced by two point correlation functions in all possible ways by Wick contraction. In the LQCD analysis, the path integral in eq. (2.31) is usually evaluated by the Monte-Carlo simulation.

2.4 Sign Problem

As I mentioned above, the lattice field theory is a powerful tool to study the field theory non-perturbatively. Especially LQCD, which makes it possible to study QCD numerically and non-perturbatively, had brought a lot of successes, e.g. a prediction of hadron masses of grand state, evaluating standard model parameters like the lambda parameter, and understanding the property of the chiral symmetries. Physicists are also interested in QCD at finite density, however LQCD approach at finite density is not available at this time. Figure 2.1 is an expected picture of the phase diagram of QCD. As shown in the figure, LQCD approach is only applicable to the region at or near the vanishing baryon chemical potential ($\mu_B = 0$ region

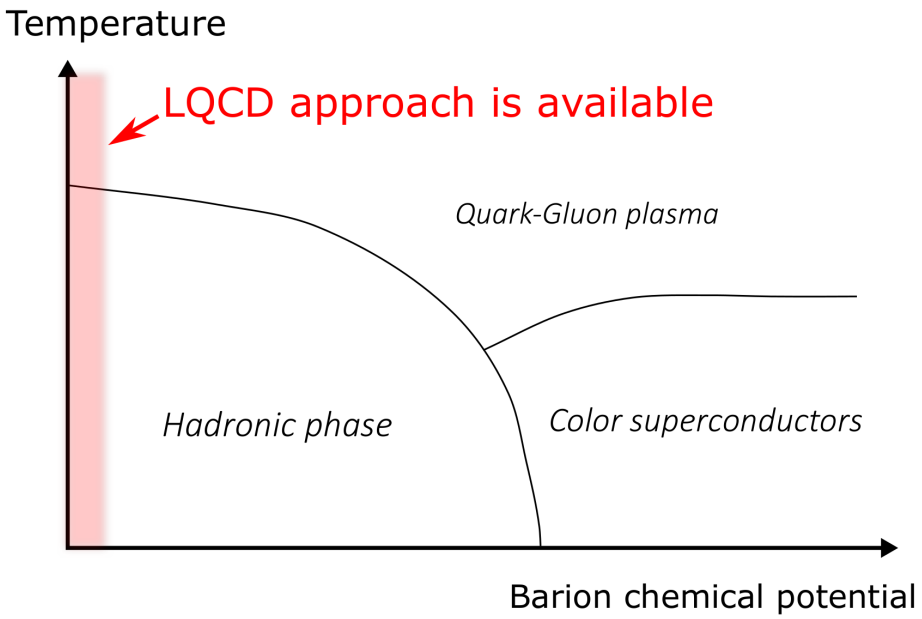

FIGURE 2.1 Phase diagram of QCD.

in the figure). At zero chemical potential, eq. (2.31) can be evaluated using the Monte Carlo method on which the standard LQCD simulations at zero or finite temperature relay as the weight $\det(D_{\mathrm{WC}})\,\mathrm{e}^{-S_{\mathrm{W}}}$ is real and non negative. When we include the baryon (or quark) chemical potential in the LQCD partition function to study the finite baryon density state of QCD, the fermion determinant $det[D_W C]$ takes complex numbers in general. In this case we cannot employ the Monte Carlo method to evaluate eq (2.31) as the weight $\det(D_{\mathrm{WC}}[U,\mu_{\mathrm{B}}])$ is complex number. Even if we could evaluate eq. (2.31) with an integration scheme (quadrature) on the multi dimensional integration $\int dU_m u(n)$ on the link variables, the complex phase from the determinant could rapidly oscillate so that the precise numerical evaluation becomes impossible due to a large cancellation. This problem is called the sign problem. To avoid the sign problem various method are proposed so far, for example the reweighting method [2], Taylor expansion method [3, 4], the method of analytic continuation from imaginary to real chemical potential [5–13], the complex Langevin method [14–16] and the Lefschetz-thimble method [17, 18]. The tensor renormalization group is one such method. In this thesis I focus on TRG and I mention the detail of TRG with the use of two dimensional Ising model in the next chapter.

3 Tensor Renormalization Group

TRG can be used to evaluate the partition function of a system on lattice very approximately and effectively when the partition function has a form of so called tensor network form. The advantage of the use of TRG is that TRG directly evaluates the partition function numerically without using any Monte Carlo method. Thus TRG is free from the sign problem. Moreover TRG has only a systematic error since a clear and computable definition of observable is given by TRG on the lattice. M. Levin and C. P. Nave proposed TRG analysis for the two dimensional Ising model [19]. Several applications of TRG to various models in the lattice field theory have been studied [20–32]. However TRG analysis has several unsolved problems. One is that the use of TRG in the higher dimensional system is still hard due to the computational cost. When we apply TRG method to an relativistic quantum field theory, which is always defined on four-dimensional lattice, the computational cost becomes quite large compared to the two-dimensional theory. Other problem is that numerical results in TRG analysis has an irregular parameter dependence. This irregular behavior causes a difficulty to evaluate the error.

In this chapter I explain TRG algorithm and its effectiveness showing some numerical results for the two-dimensional Ising model. In the next section I introduce the algorithm. The numerical results is given in the last section of this chapter. I show the properties of TRG by investigating the Helmholtz free energy and the specific heat by varying parameters of TRG.

3.1 Tensor Renormalization Group for 2D-Ising Model

I define the Hamiltonian and partition function of the two-dimensional Ising model. Then I transform the partition function into the so called tensor network form by replacing the dynamical variables form Ising spin to index. I consider a $M \times N$ finite lattice. The lattice site is labeled by $n = (n_1, n_2)$, where $n_1 = 1, 2, \ldots, M$ and $n_2 = 1, 2, \ldots, N$. The spin variable on the site n is denoted as σ_n, and its value takes ± 1. Here I consider two interactions, nearest neighbor

interaction and external field interaction. The Hamiltonian of this model is written as

$$H(\{\sigma\}) = \sum_n \left[-J_1\sigma_n\sigma_{n+\hat{1}} - J_2\sigma_n\sigma_{n+\hat{2}} - h\sigma_n\right], \tag{3.1}$$

whereJ_1, J_2 and h are coefficients of interactions, and $\hat{\mu}$ is the unit vector in the direction μ. From the Hamiltonian the partition function is,

$$\begin{aligned} Z &= \left(\prod_m \sum_{\sigma_m=\pm1}\right) \exp\left(-\beta H(\{\sigma\})\right) && (3.2)\\ &= \left(\prod_m \sum_{\sigma_m=\pm1}\right) \prod_n \exp\left(J_1\beta\sigma_n\sigma_{n+\hat{1}} + J_2\beta\sigma_n\sigma_{n+\hat{2}} + h\beta\sigma_n\right) && (3.3)\\ &= \prod_n \sum_{\sigma_n=\pm1} \exp\left(J_1\beta\sigma_n\sigma_{n+\hat{1}} + J_2\beta\sigma_n\sigma_{n+\hat{2}} + h\beta\sigma_n\right), && (3.4) \end{aligned}$$

where β is inverse of temperature T.

The first step to introduce TRG is rewriting the partition function Z in the tensor network representation (TNR),

$$Z = \sum_{i,j,k,l,\ldots} T_{i,j,k,l}T_{k,m,n,p}\cdots. \tag{3.5}$$

Figure 3.1 shows a schematic picture of TNR. Ts build the network from the lattice, and its indices behave as the link of the lattice. Note that tensors T on each site are independent on the site index n , which will be explained more explicitly in below. The contraction of the tensor in eq. (3.5) depend on the boundary condition of the lattice. In this thesis I employ the periodic boundary condition.

Here I introduce the form of T. The exponential part in eq. (3.4) can be written as

$$\begin{aligned} \mathrm{e}^{J_\mu\beta\sigma_n\sigma_{n+\hat{\mu}}} &= \cosh(J_\mu\beta\sigma_n\sigma_{n+\hat{\mu}}) + \sinh(J_\mu\beta\sigma_n\sigma_{n+\hat{\mu}}) \qquad (\mu = 1, 2)\\ &= \cosh(J_\mu\beta) + \sigma_n\sigma_{n+\hat{\mu}}\sinh(J_\mu\beta)\\ &= \cosh(J_\mu\beta)\left(1 + \sigma_n\sigma_{n+\hat{\mu}}\tanh(J_\mu\beta)\right)\\ &= \cosh(J_\mu\beta)\sum_{i_n=0}^{1}\left[\sigma_n\sigma_{n+\hat{\mu}}\tanh(J_\mu\beta)\right]^{i_n}, && (3.6)\\ \mathrm{e}^{J_\mu\beta\sigma_n} &= \cosh(h\beta) + \sigma_n\sinh(h\beta). && (3.7) \end{aligned}$$

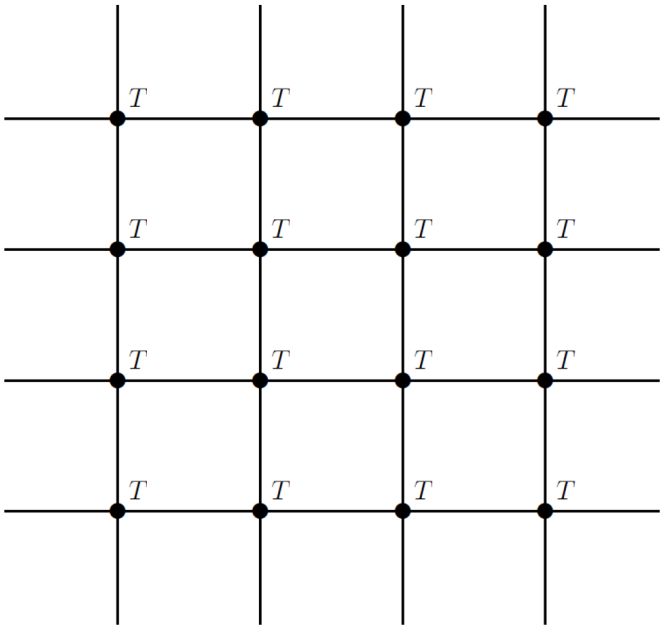

FIGURE 3.1 Picture of TNR.

Therefore I obtain the form of T as follows,

$$
\begin{aligned}
Z = \prod_n \sum_{\sigma_n=\pm1} \sum_{i_n=0,1} \sum_{j_n=0,1} \Big[& \cosh(J_1\beta)\cosh(J_2\beta) \\
& \times (\cosh(h\beta) + \sigma_n \sinh(h\beta)) \\
& \times \sigma_n^{i_n} \sigma_{n+\hat{1}}^{i_n} \sigma_n^{j_n} \sigma_{n+\hat{2}}^{j_n} \tanh(J_1\beta)^{i_n} \tanh(J_2\beta)^{j_n} \Big] \qquad (3.8) \\
= \prod_n \sum_{\sigma_n=\pm1} \sum_{i_n=0,1} \sum_{j_n=0,1} \Big[& \cosh(J_1\beta)\cosh(J_2\beta) \\
& \times (\sigma_n^{i_n+i_{n-\hat{1}}+j_n+j_{n-\hat{2}}} \cosh(h\beta) + \sigma_n^{i_n+i_{n-\hat{1}}+j_n+j_{n-\hat{2}}+1} \sinh(h\beta)) \\
& \times \tanh(J_1\beta)^{\frac{i_n+i_{n-\hat{1}}}{2}} \tanh(J_2\beta)^{\frac{j_n+j_{n-\hat{2}}}{2}} \Big] \qquad (3.9) \\
= \prod_n \sum_{i_n=0,1} \sum_{j_n=0,1} \Big[& 2\cosh(J_1\beta)\cosh(J_2\beta)\cosh(h\beta) \tanh(J_1\beta)^{\frac{i_n+i_{n-\hat{1}}}{2}} \tanh(J_2\beta)^{\frac{j_n+j_{n-\hat{2}}}{2}} \\
& \times \delta_{(i_n+i_{n-\hat{1}}+j_n+j_{n-\hat{2}}) \bmod 2,0} \\
& + 2\cosh(J_1\beta)\cosh(J_2\beta)\sinh(h\beta) \tanh(J_1\beta)^{\frac{i_n+i_{n-\hat{1}}}{2}} \tanh(J_2\beta)^{\frac{j_n+j_{n-\hat{2}}}{2}} \\
& \times \delta_{(i_n+i_{n-\hat{1}}+j_n+j_{n-\hat{2}}) \bmod 2,1} \Big] \qquad (3.10) \\
\equiv \prod_n \sum_{i_n=0,1} \sum_{j_n=0,1} & T_{i_n,j_n,i_{n-\hat{1}},j_{n-\hat{2}}} \qquad (3.11)
\end{aligned}
$$

The TNR form of eq.(3.11) is exactly identical to the original partition function (3.2) and there is no computational benefit from (3.11) when all the summation on the bond indexes (i_n, j_n) are taken exactly. Note that the tensor with four legs T_{ijkl} does not depend on the site index n. The system size N and M is simply involved in the number of tensors contained in the tensor products. TRG approximates the summation on the bond indexes by recursively taking the partial tensor products around a site followed by an approximation on the resulting tensor reducing the bond degree of freedom. The reduction of the degree of the bond index of a tensor is achieved by applying the singular value decomposition (SVD) on the tensor. Before applying SVD on tensor with four legs, I briefly explain the SVD for a matrix and the approximation. SVD theorem states that a $M \times N$ matrix A can be decomposed as

$$A_{i,j} = \sum_{m=1}^{M} \sum_{n=1}^{N} U_{i,m} \Lambda_{m,n} V^{\dagger}_{n,j}, \tag{3.12}$$

where Λ is a $M \times N$ diagonal matrix, and U and V are the $M \times M$ and $N \times N$ unitary matrices, respectively. The singular values $\lambda_1, \lambda_2, \ldots, \lambda_{\min(M,N)}$ are assigned on the diagonal component of Λ, $\Lambda = \mathrm{diag}\left(\lambda_1, \lambda_2, \ldots, \lambda_{\min(M,N)}, 0, \ldots\right)$. We assume that the magnitude of the singular values $lambda_k$ have a hierarchy, and it is ordered as $\lambda_1 > \cdots$. In this case we can approximate the matrix A with a low lank diagonal components by dropping the minor components from the SVD. When the singular values have a large gap at $\lambda_{D_cut} \gg \lambda_{D_cut+1}$, we can approximate A very precisely as

$$A_{i,j} \simeq \sum_{m=1}^{D_{\mathrm{cut}}} \sum_{n=1}^{D_{\mathrm{cut}}} U_{i,m} \Lambda_{m,n} V^{\dagger}_{n,j} \tag{3.13}$$

$$= \sum_{k}^{D_{\mathrm{cut}}} U_{i,k} \lambda_k V^{\dagger}_{k,j}. \tag{3.14}$$

Using the SVD, we can approximate T as

$$T_{i,j,k,l} \simeq \begin{cases} \sum_{a=1}^{D_{\mathrm{cut}}} U_{(i,j),a} \lambda_a V^{\dagger}_{a,(k,l)} \\ \sum_{a=1}^{D_{\mathrm{cut}}} \overline{U}_{(l,i),a} \overline{\lambda}_a \overline{V}^{\dagger}_{a,(j,k)}. \end{cases} \tag{3.15}$$

Here we assume that the singular values of the matrix constructed from the tensor has the desired gap at D_{cut}. To construct a matrix from a tensor with four legs, there are several combinations in grouping the indexes. Two forms in eq. (3.15) are used to take partial contraction of four tensors. In Figure 3.2 shows the tensor

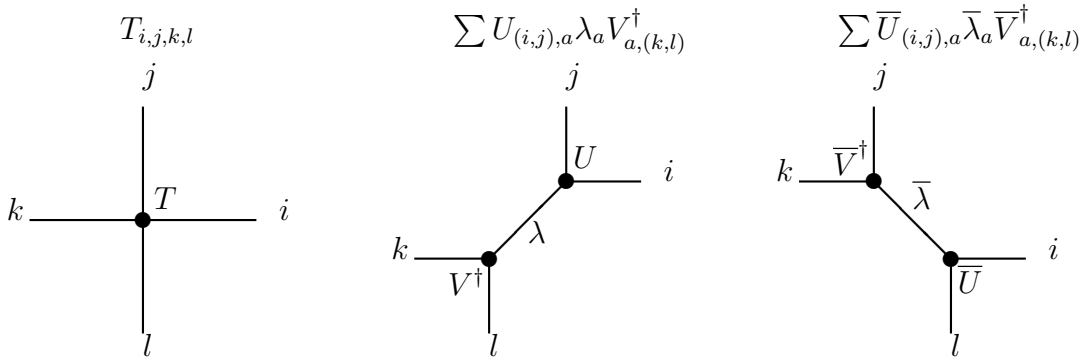

FIGURE 3.2 The diagram of SVD for T.

network diagrams before and after the SVD of a T. From the singular value λ_k and $\overline{\lambda}_k$, and corresponding matrix U, $\overline{U}$, $\overline{V}$ and $\overline{V}$, one obtains a new tensor W,

$$W_{a,b,c,d} \equiv \sum_{i,j,k,l=1}^{\chi} \left(U_{(i,j),a}\sqrt{\lambda_a}\right)\left(\overline{U}_{(j,k),b}\sqrt{\overline{\lambda}_b}\right)\left(\sqrt{\lambda_c}V^\dagger_{c,(k,l)}\right)\left(\sqrt{\overline{\lambda}_d}\overline{V}^\dagger_{d,(l,i)}\right), \quad (3.16)$$

where χ is the degrees of freedom of the subscript i, j, k, l of $T_{i,j,k,l}$. New TNR is defined by the new tensor W, and figure 3.3 shows the diagram. The approximation introduced by the cut $D_{\rm cut}$ reduces the degree of freedom of the bond indexes on the new tensor W at $D_{\rm cut}$ as $a, b, c, d \in [1, \ldots, D_{\rm cut}]$. The scale of the new TNR is that $1/\sqrt{2}$ times the original scale. It is corresponding to the renormalization of the scale of the lattice. Repeating the above procedure, the partition function is can be written by the contraction on by four tensors,

$$Z = \sum_{i,j,k,l,m,n,o,p} X_{i,j,k,l}X_{k,m,i,n}X_{p,n,o,m}X_{o,l,p,j}. \quad (3.17)$$

If we employ $D_{\rm cut}$ in the last SVD approximation in the iteration, the computational cost of the last truncation in eq (3.17) is about $O(D^6_{\rm cut})$.

3.2 Numerical Results

I explained the TRG algorithm and give the form of the partition function to compute by TRG in the previous section. Here I show several numerical results for two dimensional Ising model obtained by the use of TRG. In this thesis I set parameters in Hamiltonian (3.1) to $J_1 = J_2 = 1$ and $h = 0$.

Figure 3.4 shows the computation time of TRG algorithm against the cutoff $D_{\rm cut}$ for several $V = (L/a)^2$ lattice. The vertical axis is the system time divided by $D^6_{\rm cut}$. The lattice size effect for the computation time , which is proportional to the

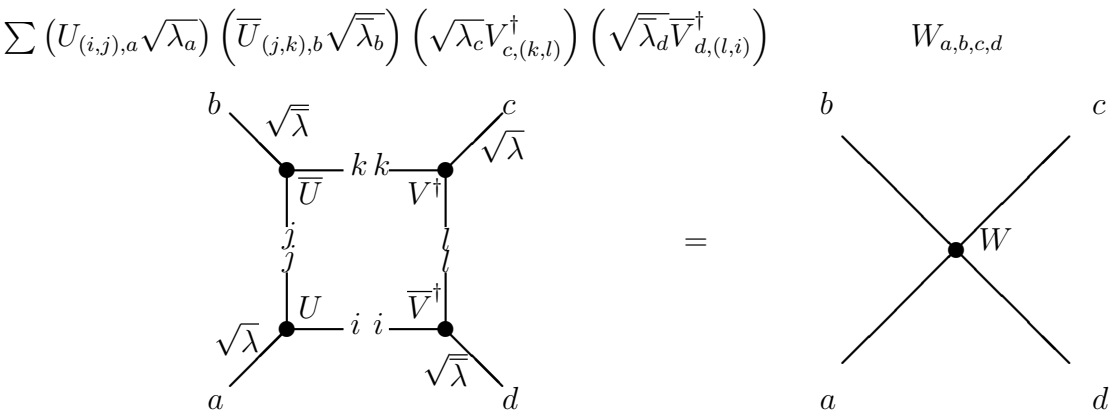

FIGURE 3.3 The diagram of the construction of W.

logarithmic function of the lattice size, is dominant for small $D_{\rm cut}$s, but for large $D_{\rm cut}$s the computation time behaves $O(D_{\rm cut}^6)$. The above behavior is consistent with the analytic accounting of the computational cost of eq. (3.17).

Figure 3.5 shows the typical behavior of the singular value. The singular values in this figure are obtained from the course grained tensor after four TRG steps. The singular values are sorted by the order of magnitude, and labeled by the serial number. The vertical axis is the singular value normalized by the maximum singular value, and the horizontal axis is the serial number. One can find the degeneracy in the singular values which structure will be more closely investigated in the next chapter.

Once the partition function is obtained, from which we can extract any thermodynamic observables. Here I calculate the Helmholtz free energy F and the specific heat C_V, wchich is obtained by the numerical derivative of Z, as examples,

$$F \equiv -\frac{1}{V\beta}\log(Z), \tag{3.18}$$

$$C_V = -\beta^2 \frac{\partial^2}{\partial\beta^2}\left(\beta F\right). \tag{3.19}$$

For the two dimensional Ising model there is the exact solution given in [43,44], then we can compare the numerical results with the exact solutions. Figure 3.6 shows the temperature dependence of the free energy density simulated on $V = (2^{16})^2$ lattice for several $D_{\rm cut}$. The black solid line is the exact solution, and the black dotted line denotes the exact solution of the critical temperature of the two dimensional Ising model, $T_{\rm c}^{\rm exact} = 2/[\log(1+\sqrt{2})] = 2.2691853\cdots$. Increased $D_{\rm cut}$, the numerical results obtained by TRG are approaches the exact solution. Especially for $D_{\rm cut} \geq 4$ the relative error of the free energy is the order of 10^{-5}. Examples of the value of

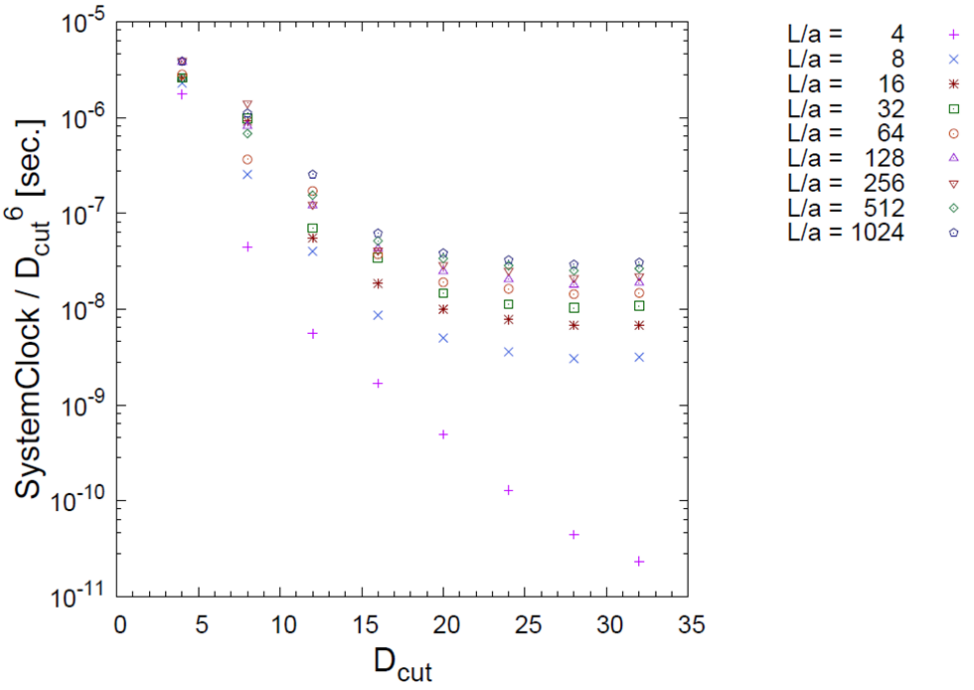

FIGURE 3.4 Computation time to obtain Z by TRG.

the free energy obtained by using TRG algorithm at $\beta = 0.35$ for several lattices and D_{cut} are in table 3.1. Comparing the numerical results of F with the exact solutions, which are written in parentheses in the table, one can see that the TRG yields quite precise approximations to the free energy, e.g. the result for $D_{\text{cut}} = 32$ on $V = (1024)^2$ lattice is consistent within 8-digit. Figure 3.7 shows the temperature dependence of the specific heat C_V evaluated on $V = (1024)^2$ lattice for several D_{cut}s. The black solid line is the exact solution, and the black dotted line denotes the exact T_{c}. In this figure one can see that the position of the sharp peaks converge to the exact critical temperature as increasing D_{cut}. Fluctuations shown in the figure is caused due to the irregular parameter dependence which is looked more closely in the next chapter. Figure 3.8 shows the temperature dependence of the specific heat obtained by TRG for $D_{\text{cut}} = 32$ on several lattices. The black solid line is the exact solution, and the black dotted line denotes the exact T_{c}. From this figure one can see that the result on the lattice with larger volume is closer to the exact solution for the infinite volume.

The transition temperature T_{c} is evaluated from the peak position of the specific heat C_V. Figure 3.9 shows the D_{cut} dependence of the transition temperature T_{c} evaluated on the $V = (1024)^2$ lattice. The black points and the solid line are the results obtained from TRG analysis, and the horizontal dashed line denotes the exact solution of the critical temperature $T_{\text{c}}^{\text{exact}}$. As one can see in the figure, the

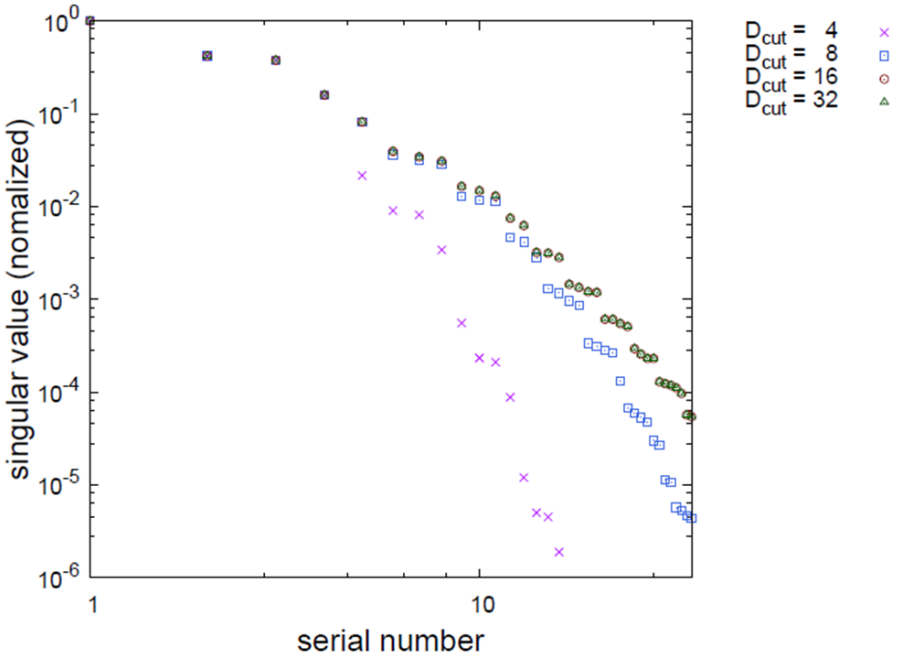

FIGURE 3.5 Typical behavior of the singular value.

results for the sufficiently large D_{cut} approach the exact solution.

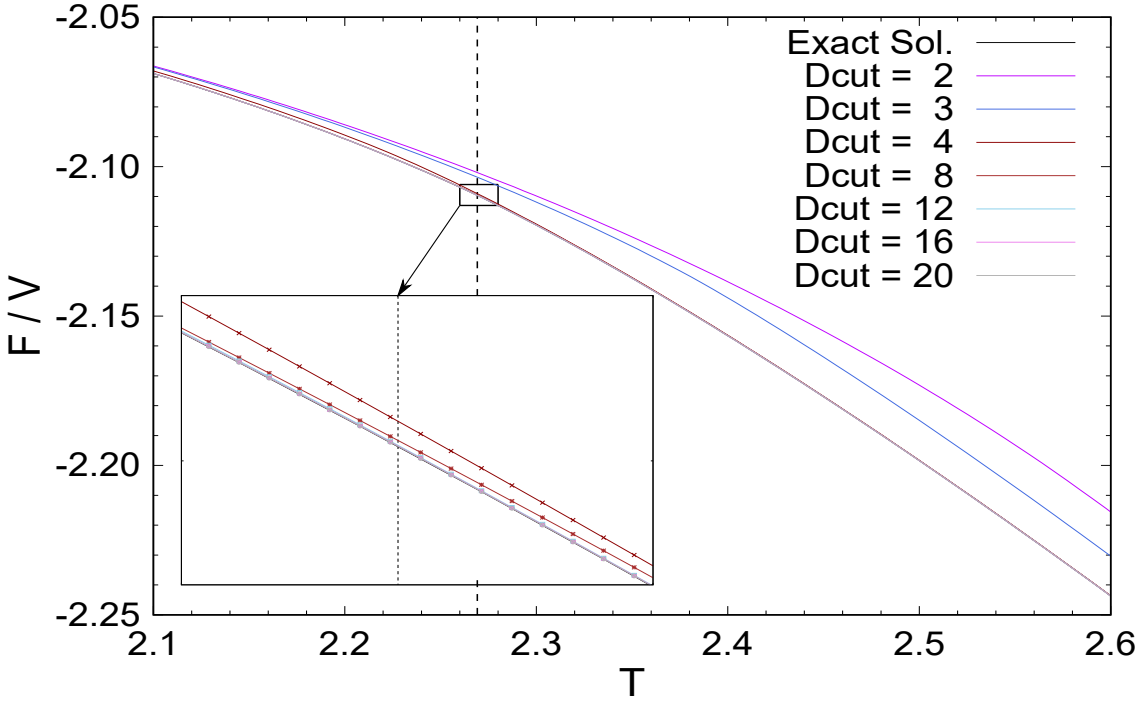

FIGURE 3.6 Free energy density F/V on $V = (2^{16})^2$ lattice.

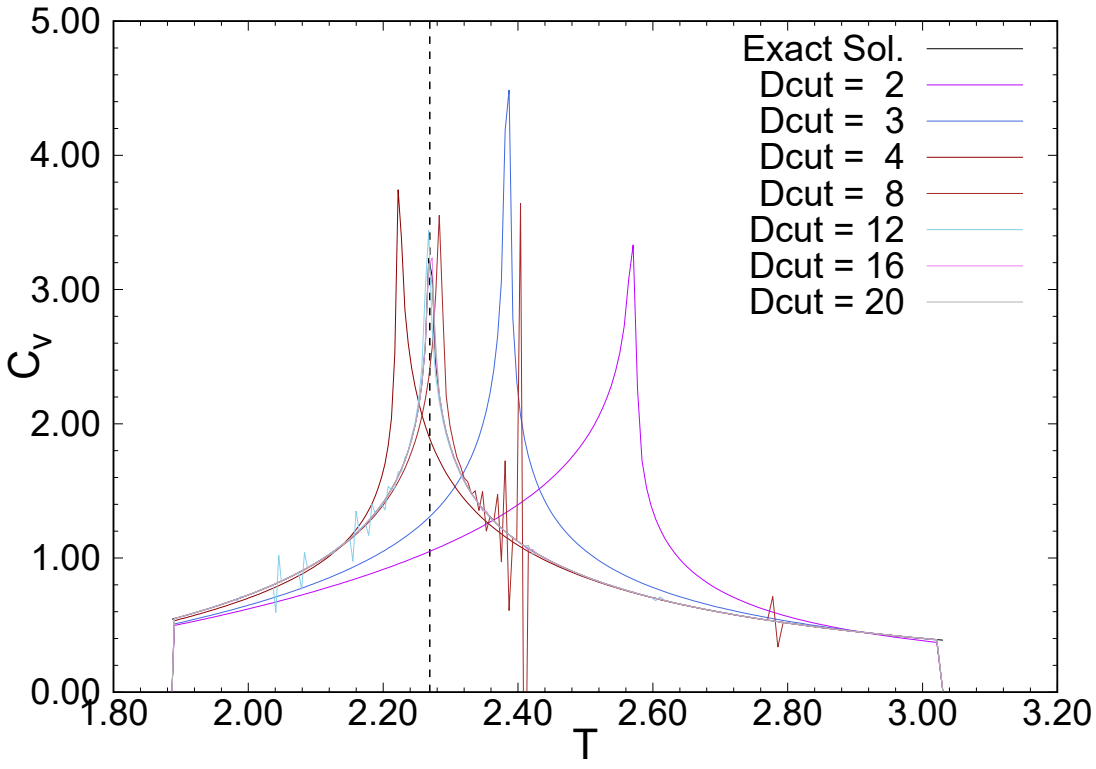

FIGURE 3.7 Specific heat C_V for several D_{cut}s obtained by TRG on $V = (1024)^2$ lattice.

TABLE 3.1 Comparison table of the free energy F. The simulation is done for $\beta = 0.35$. Values in parentheses are the exact solution given in [44].

V	D_{cut}	F	V	D_{cut}	F
$(4)^2$	4	-2.4222181375925	$(128)^2$	4	-2.3714194439588
	8	-2.4222181375925		8	-2.3714328162421
	16	-2.4222181375925		16	-2.3714819994446
	32	-2.4222181375925		32	-2.3714822244363
		(-2.4222181375925)			(-2.3714822353167)
$(8)^2$	4	-2.3744926368303	$(256)^2$	4	-2.3714194439588
	8	-2.3749307990750		8	-2.3714328162417
	16	-2.3749713762661		16	-2.3714819994445
	32	-2.3749713762661		32	-2.3714822244363
		(-2.3749713762660)			(-2.3714822353167)
$(16)^2$	4	-2.3714400743885	$(512)^2$	4	-2.3714194439588
	8	-2.3714810565284		8	-2.3714328162415
	16	-2.3715309388402		16	-2.3714819994444
	32	-2.3715311887095		32	-2.3714822244363
		(-2.3715311978132)			(-2.3714822353167)
$(32)^2$	4	-2.3714194462786	$(1024)^2$	4	-2.3714194439588
	8	-2.3714328351104		8	-2.3714328162415
	16	-2.3714820305271		16	-2.3714819994444
	32	-2.3714822561175		32	-2.3714822244363
		(-2.3714822671500)			(-2.3714822353167)
$(64)^2$	4	-2.3714194439588			
	8	-2.3714328162440			
	16	-2.3714819994457			
	32	-2.3714822244364			
		(-2.3714822353168)			

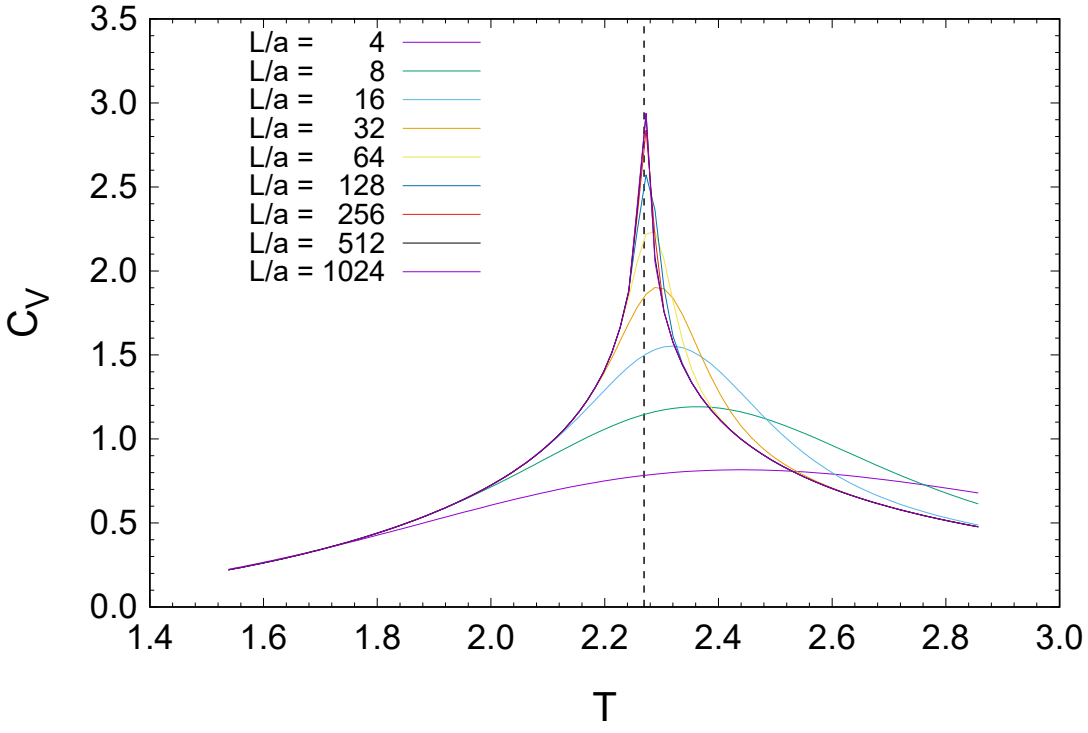

FIGURE 3.8 Specific heat C_V on several lattices obtained by TRG for $D_{\rm cut} = 32$.

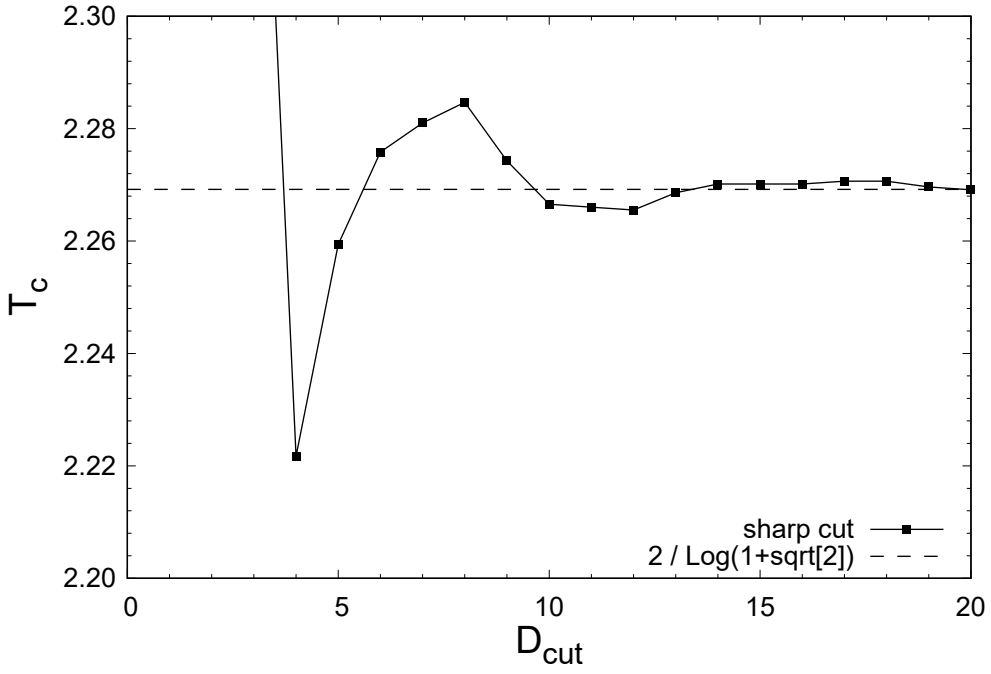

FIGURE 3.9 Transition temperature $T_{\rm c}$ evaluated on the $V = (1024)^2$ lattice.

4 Simulations and Results

In this chapter I focus on a problem of TRG analysis, then I propose and test an improvement idea to avoid this problem.

4.1 Irregular Behavior in TRG Analysis

In figure 3.7 shown in section 3.2, the irregular behavior arise as the fluctuation of the result. I focus on this irregular behavior in my work. In this section I identify the origin of this behavior and propose an idea of the improvement of TRG algorithm to avoid this problem.

4.1.1 Crossover of Singular Values

Here I consider a cause of the above problem. I expect that the cause is crossover of singular values at $D_{\rm cut}$. Eq. (3.15) can be rewritten as the form,

$$T \simeq \sum_{m=1}^{D_{\rm cut}} \lambda_m [\vec{u}_m]^{\rm T} \vec{v}_m \equiv T^{(1)}, \tag{4.1}$$

where $\vec{u}_m$ and $\vec{v}_m$ are the left and right singular vector related to λ_m, respectively. If Nth and N'th singular values are degenerated, $\lambda_N \sim \lambda_{N'}$, Nth and N'th left and right singular vectors, $\vec{u}_N$, $\vec{u}_{N'}$, $\vec{v}_N$ and $\vec{v}_{N'}$, are commutative. Here I assume $N > N'$. The crossover of the singular vectors is not important when $D_{\rm cut} \neq N$. However if $D_{\rm cut} = N$, and $\vec{u}_N \neq \vec{u}'_N$ and $\vec{v}_N \neq \vec{v}'_N$, the crossover affects the final result.

Actually the effect of the crossover is observed in Figure 4.1. This figure shows the temperature dependence of the relative residual of the free energy F obtained by TRG simulations on the $V = (16)^2$ lattice with $D_{\rm cut} = 8, 12, 16, 20$. In this figure, one can find some discontinuity points. It seems that there is no systematic tendency on the location of the discontinuity points to the temperature and $D_{\rm cut}$. These discontinuity points causes an unexpected behavior shown in Figure 4.2, which is an Internal energy obtained by the numerical derivative of the free energy. The irregular

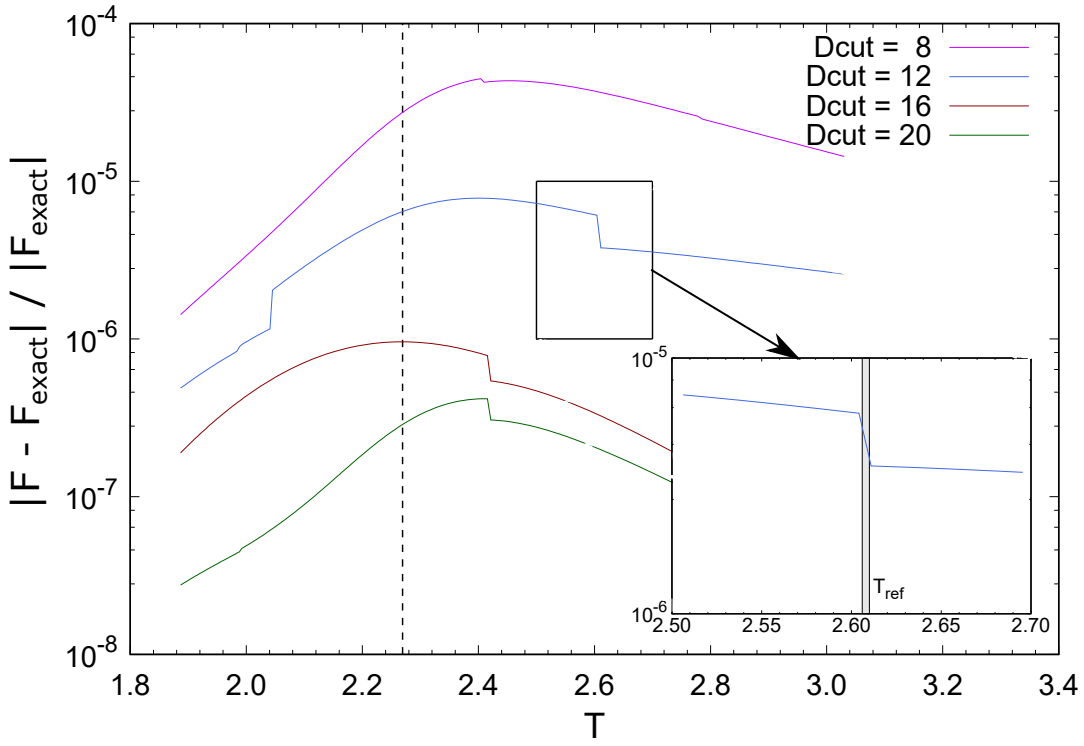

FIGURE 4.1 Temperature dependence of the relative residual of the free energy F evaluated for $D_{\rm cut} = 8, 12, 16, 20$ on $V = (16)^2$ lattice. The gray band in an enlarged figure at the bottom right is the temperature which the irregular behavior is caused.

behavior in terms of "T" may lead one to misidentify a important observable like a critical point. Avoiding to misidentify the observable, it is important to study an origin and treatment of the discontinuity point. In order to see the origin of these discontinuities , I trace the singular values near $D_{\rm cut}$ around the discontinuity and found that level crossing occurs at $D_{\rm cut}$ and the discontinuity temperature as a function of inverse temperature as described above.

For example I show a case with the discontinuity point on $T_{\rm ref} \sim 2.608$ for $D_{\rm cut} = 12$ simulation which case is magnified in figure 4.1. In this case, the crossover behavior at $D_{\rm cut} = 12$ occurs in the 6th SVD. The singular values λ_{12} and λ_{13} almost degenerates and the replacement of singular vectors occurs when the temperature cross $T_{\rm ref}$. The important point in this level crossing is the singular vectors are completely different each others as,

$$\begin{aligned} \vec{u}_{12}^{(T<T_{\rm ref})} &\neq \vec{u}_{13}^{(T>T_{\rm ref})}, \quad \vec{u}_{12}^{(T>T_{\rm ref})} \simeq \vec{u}_{13}^{(T<T_{\rm ref})}, \\ \vec{v}_{12}^{(T<T_{\rm ref})} &\neq \vec{v}_{13}^{(T>T_{\rm ref})}, \quad \vec{v}_{12}^{(T>T_{\rm ref})} \simeq \vec{v}_{13}^{(T<T_{\rm ref})}, \end{aligned} \tag{4.2}$$

even with the degenerate singular values. Thus the numerical value of $T^(1)$ (eq. (4.1)) approximated by the SVD with $D_{\rm cut}$ shows the discontinuity when the temperature cross $T_{\rm ref}$. Here, in the case of $V = (16)^2$ lattice, SVD is done 6 times until

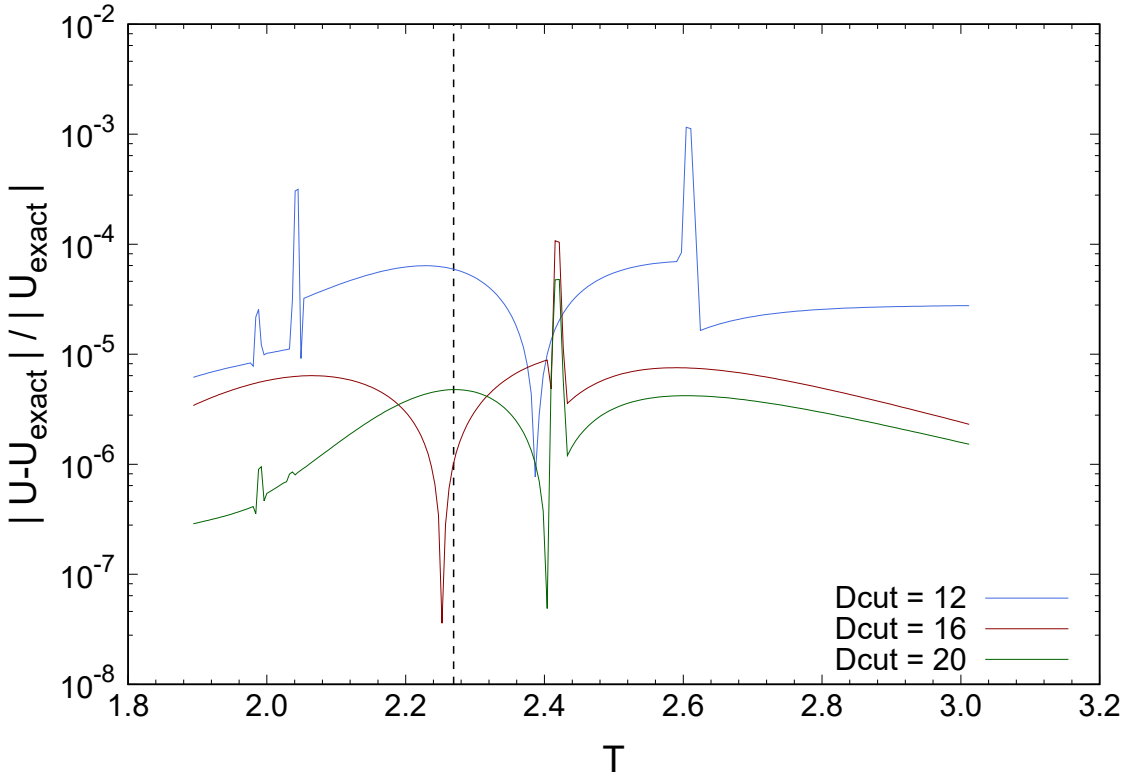

FIGURE 4.2 Temperature dependence of the relative residual of the Internal energy evaluated for $D_{\rm cut} = 8, 12, 16, 20$ on $V = (16)^2$ lattice.

I compute the contraction of tensor.

Figure 4.3 shows the crossover between the 12th singular value and 13th. Open and Filled circles in $T < T_{\rm ref}$ are the singular values for λ_{12} and λ_{13}, respectively. When T becomes higher than $T_{\rm ref}$, the ordering of singular values is interchanged so that open circles are for λ_{13} and filled circles are for λ_{12}.

Here I show that the discontinuity points in figure 4.1 does not arise when the above interchanging of singular values around $T_{\rm ref}$ is not caused. In order to clarify the effect of the crossover on the free energy, I introduce the following SVD approximation, ,

$$T^{(2)} = \begin{cases} T^{(1)} & \text{for } T < T_{\rm ref}, \\ \displaystyle\sum_{m=1}^{D_{\rm cut}-1} \lambda_m [\vec{u}_m]^{\rm T} \vec{v}_m + \lambda_{D_{\rm cut}+1} [\vec{u}_{D_{\rm cut}+1}]^{\rm T} \vec{v}_{D_{\rm cut}+1} & \text{for } T \geq T_{\rm ref}, \end{cases} \tag{4.3}$$

$$T^{(3)} = \begin{cases} \displaystyle\sum_{m=1}^{D_{\rm cut}-1} \lambda_m [\vec{u}_m]^{\rm T} \vec{v}_m + \lambda_{D_{\rm cut}+1} [\vec{u}_{D_{\rm cut}+1}]^{\rm T} \vec{v}_{D_{\rm cut}+1} & \text{for } T < T_{\rm ref}, \\ T^{(1)} & \text{for } T \geq T_{\rm ref}. \end{cases} \tag{4.4}$$

The replacement of singular pairs at $T_{\rm ref}$ and $D_{\rm cut}$ is removed by hand in these tensor approximations.

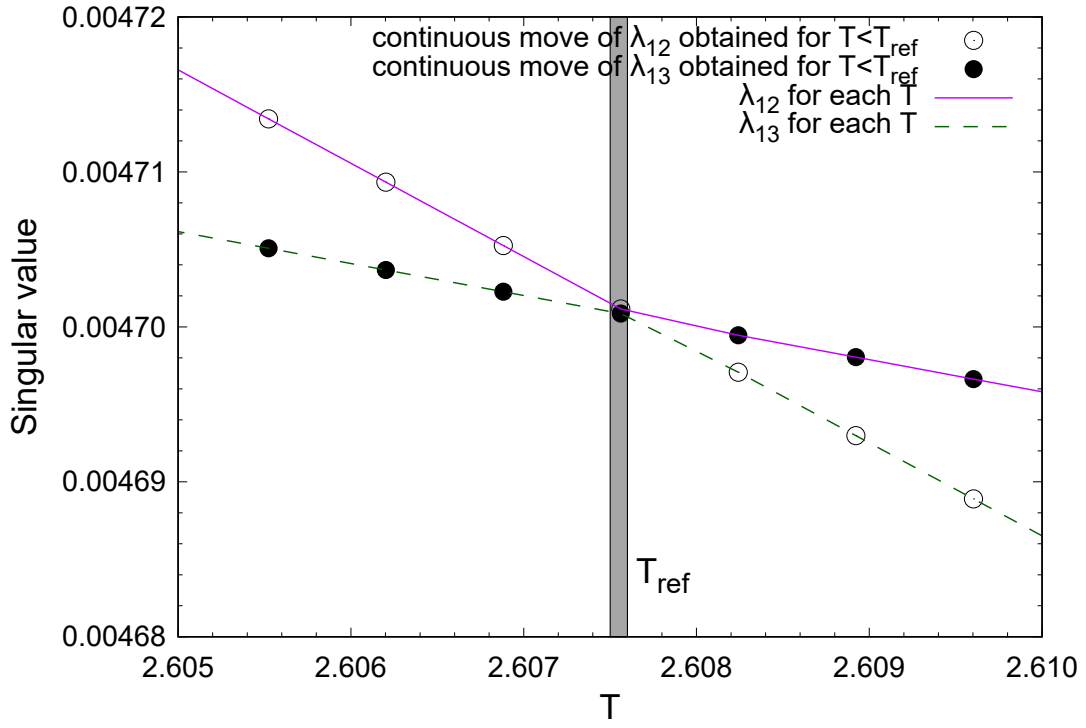

FIGURE 4.3 Crossover between the 12th singular value and 13th one obtained in the course of TRG analysis for $D_{\rm cut} = 12$ on the $V = (16)^2$ lattice. The gray band is the temperature which the irregular behavior is caused. See text for lines and points.

Figure 4.4 is a comparison among three simulations obtained from the each definition $T^{(1)}$, $T^{(2)}$ and $T^{(3)}$. The blue dashed line corresponds to the original result with $T^(1)$, while green and cyan thick lines are results with $T^(2)$ and $T^(3)$, respectively. From this figure, we can see that the discontinuity disappears with $T^(2)$ and $T^(3)$ for which the replacement of singular pairs in the approximation is absent. Thus I confirm the origin of discontinuity is in the SVD approximation when the crossover of degenerated singular pairs occurs crossing the temperature.

In the next subsection I propose a method to suppress this discontinuity.

4.1.2 Introduction of Smooth cutoff

In the previous subsection, I investigated the crossover effect of the singular vector. This problem is caused by the sharp cutoff at *Dcut* in eq. (3.15), where the singular vectors are completely replaced over $T_{\rm ref}$. I call this conventional method as "sharp cutoff method". We can generalize the approximation by introducing a weight factor in the SVD decomposition as

$$T_{i,j,k,l} \simeq \sum_{m=1}^{\chi} U_{(i,j),m} \lambda_m V^{\dagger}_{m,(k,j)} w_m, \tag{4.5}$$

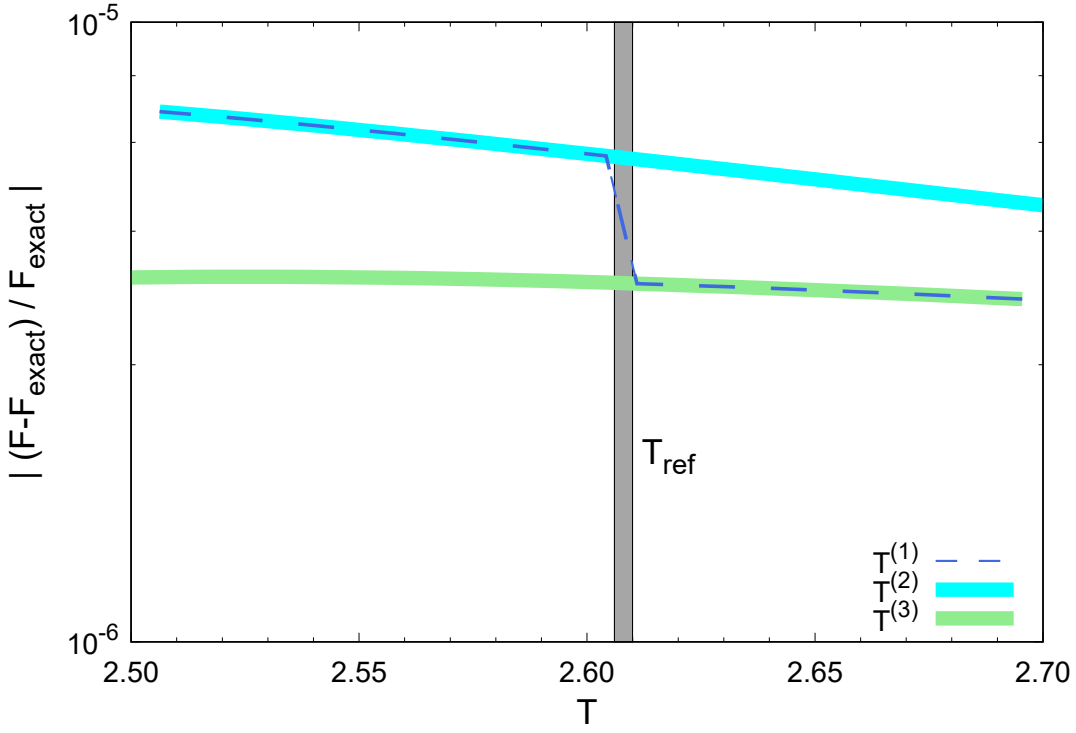

FIGURE 4.4 Comparison of the temperature dependence of the relative residue of the free energy obtained from the definition $T^{(1)}$, $T^{(2)}$ and $T^{(3)}$ with $D_{\rm cut} = 12$ on $V = (16)^2$ lattice.

where w_m is the weight factor. The sharp cutoff method corresponds to

$$w_m = \begin{cases} 1 & \text{for } (m = 1, 2, ..., D_{\rm cut}) \\ 0 & \text{for } m = D_{\rm cut} + 1, ..., \chi \end{cases} . \tag{4.6}$$

Similarly we introduce the same weight factor for the SVD approximation with $\bar{U}, \bar{V}, \bar{\lambda}$. This method might not pick entirely the important part in Z which should be considered with same extent. To avoid this problem I propose to introduce a smooth cutoff method. The idea is that if the weight factor w for singular values decrease gradually in some region, the crossover effect is mitigated and $D_{\rm cut}$ dependence of the result which computed by TRG simulation becomes smooth.

In this work I propose two types of smooth-cut: (A) a slanting cutoff and (B) a Fermi distribution function like cutoff (a FDF-cut). (A) The slanting cutoff is defined as the form which corresponds to eq. (3.15),

$$T_{i,j,k,l} \simeq \begin{cases} \sum_{m=1}^{D_{\rm cut}} U_{(i,j),m} w_m^{(\rm A)} \lambda_m V^{\dagger}_{m,(k,l)} \\ \sum_{m=1}^{D_{\rm cut}} \overline{U}_{(l,i),m} w_m^{(\rm A)} \overline{\lambda}_m \overline{V}^{\dagger}_{m,(j,k)}, \end{cases} \tag{4.7}$$

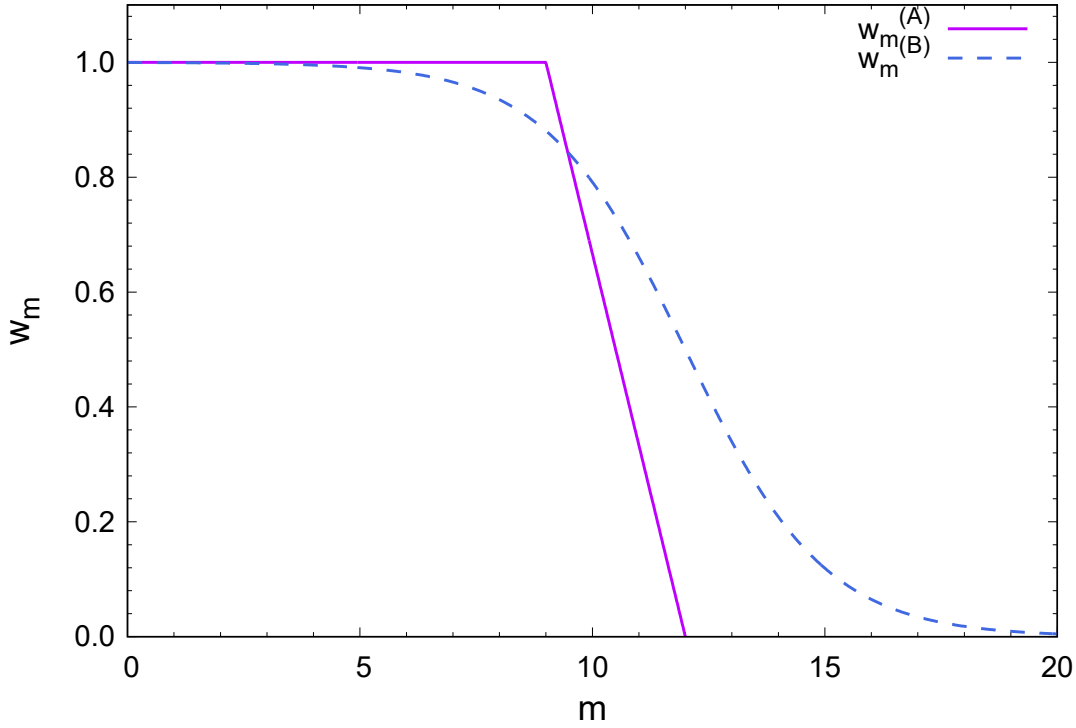

FIGURE 4.5 Wight factors $w_m^{(\mathrm{A})}$ and $w_m^{(\mathrm{B})}$.

where $w_m^{(\mathrm{A})}$ is the weight factor defined by

$$w_m^{(\mathrm{A})} = \begin{cases} 1 & (1 \leq m \leq D_{\mathrm{cut}}) \\ \frac{(D_{\mathrm{cut}}+\Delta)-m}{\Delta} & (D_{\mathrm{cut}} < m \leq D_{\mathrm{cut}}+\Delta) \end{cases}. \tag{4.8}$$

Delta is the width of the weight in which the factor linearly decreases from unity to zero. (B) The FDF cutoff is defined as the form which corresponds to eq. (3.15),

$$T_{i,j,k,l} \simeq \begin{cases} \sum_{m=1}^{D_{\mathrm{cut}}} U_{(i,j),a} w_m^{(\mathrm{B})} \lambda_m V^{\dagger}_{m,(k,l)} \\ \sum_{m=1}^{D_{\mathrm{cut}}} \overline{U}_{(l,i),a} w_m^{(\mathrm{B})} \overline{\lambda}_m \overline{V}^{\dagger}_{m,(j,k)}, \end{cases} \tag{4.9}$$

where the weight factor is defined as the form,

$$w_m^{(\mathrm{B})} = \frac{1}{\mathrm{e}^{(m-D_{\mathrm{cut}})/\sigma}+1}, \tag{4.10}$$

where σ is the extent to which the weight factor $w_m^{(\mathrm{B})}$ is squeezed. I show the shape of the wight factors $w_m^{(\mathrm{A})}$ and $w_m^{(\mathrm{B})}$ in figure 4.5. In the next section, I test these smooth cutoff methods.

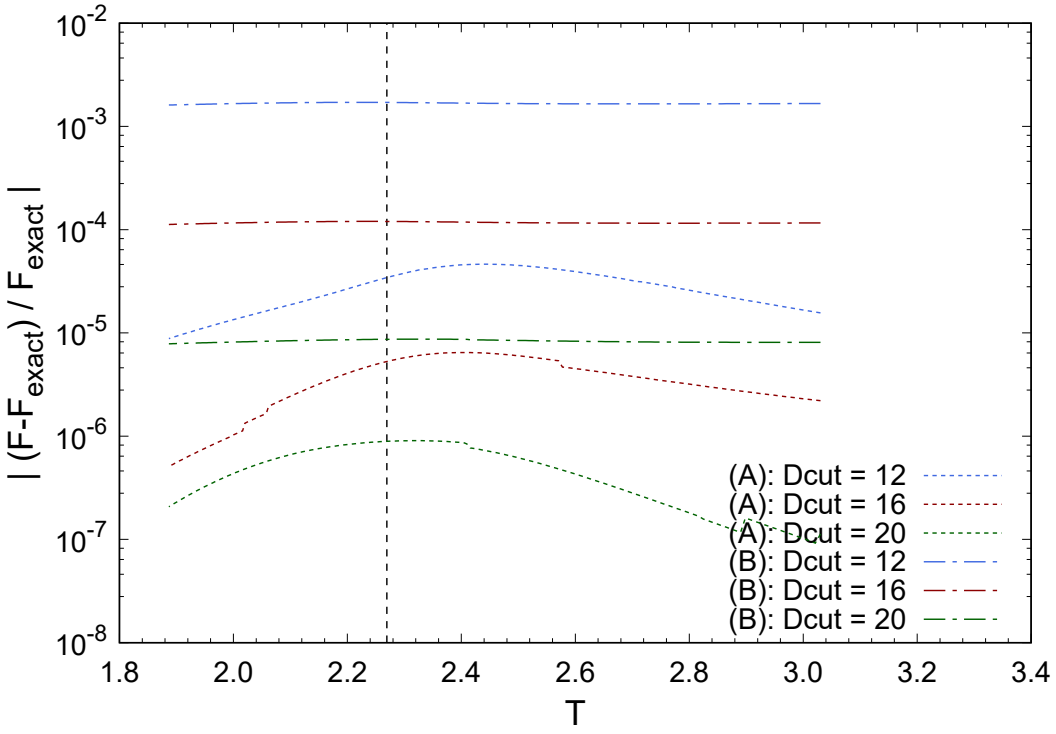

FIGURE 4.6 The relative residual of the free energy for several $D_{\rm cut}$s obtained by using $w_m^{(\rm A)}$ and $w_m^{(\rm B)}$ on $V = (16)^2$ lattice.

4.2 Numerical Results

I test the TRG with two types of smooth cutoffs, eqs. (4.7) and (4.9), on $V = (16)^2$ lattice. The parameters for the weight factors are $\Delta = 3$ and $\sigma = 1$ for the slanting cutoff (A) and the FDF cutoff (B), respectively. Figure 4.6 shows the relative residual of the free energy obtained with $w_m^{(\rm A)}$ and $w_m^{(\rm B)}$. The dotted and dash-dot lines are for the results from (A) and from (B), respectively. Comparing this figure and figure 4.1, we can see that the irregular discontinuities are well suppressed with the smooth cutoff methods. A smoother T dependence of observable like an internal energy are obtained by using smooth cutoff methods, since a numerical derivative of a smoother F in terms of T are evaluated safer. Figure 4.7 shows the relative residual of the Internal energy for several $D_{\rm cut}$s obtained by using the smooth cutoff method (B) on $V = (16)^2$ lattice. Although several small jumps still survive, a smoother T dependence of the internal energy are observed compared with figure 4.2. It imposes that the smooth cutoff scheme is effective to avoid the unexpected behavior in the result obtained by sharp cutoff scheme.

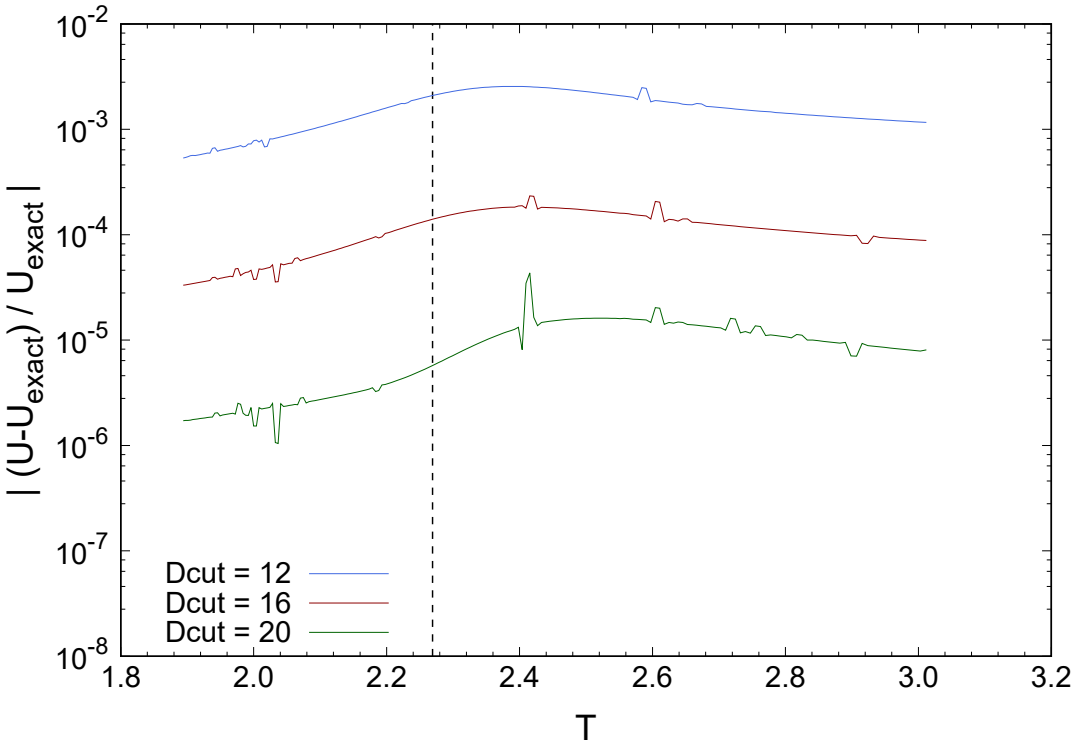

FIGURE 4.7 The relative residual of the Internal energy for several D_{cut}s obtained by using $w_m^{(\text{B})}$ on $V = (16)^2$ lattice.

5 Summary and Outlook

In the field of particle physics, Lattice QCD has became one of the most important tool and brought a lot of successful contribution to understand the physics of QCD. Although hadron masses of grand state and any other observables are computable with good accuracy by using LQCD approach, the analysis at finite density is still hard due to the sign problem. Various methods are proposed to solve this problem, and recently TRG, which is unrelated to the sign problem, is receiving a lot of attention and studied.

Using TRG analysis, the numerical evaluation of the partition function is possible when the tensor network representation is available for the target system. Especially when the spatial dimension of the system is lower, more precisely in two-dimension, the TRG method works very effectively and the approximation is quite accurate even at the critical point of the system. However the application of TRG analysis to the field theory is still hard because the computational cost grows exponentially as increasing the system dimension. Another difficulty of the TRG is the systematic control of the truncation error from the cutoff in the singular value decomposition approximation, namely the effect of D_{cut}. As shown in this thesis with the two-dimensional Ising model as an example, the cutoff introduces uncontrollable discontinuity in the free energy. This discontinuity behavior makes the systematic analysis of the phase transition or thermo dynamics properties difficult before knowing the detailed property of a target system. Because quantum field theories typically defined in four-dimension space-time, we have to employ TRG with a lower cut off to have lower computational cost. However its thermodynamic properties are not known a priori, the discontinuity introduced by the lower cutoff may spoil the quality of results obtained with TRG.

In this thesis, I focused on the discontinuity caused by the cutoff and uncovered the nature of the discontinuity using the two-dimensional Ising model. I showed that this irregular behavior is caused by the crossover of the singular values in approximating the tensor with truncated SVD. Having identified the origin of the discontinuity, I proposed the smooth cutoff method and tested the method. I confirmed that the smooth cutoff method actually works to relax the discontinuity in the free energy. On the other hand the precision of the numerical result obtained with the smooth

cutoff are decreased in comparison to the result with the same computational cost for the sharp cutoff method. This is because the smooth cutoff method is a rough approximation than the sharp cutoff method. Further improvement is expected to realize the controllable irregular parameter dependence with good accuracy in the future.

Acknowledgments

First of all, I would like to thank my supervisor, Ken-Ichi Ishikawa, for his support, guidance and patience. I also want to thank Prof. Yoshinobu Kuramashi at University of Tukuba and Dr. Daisuke Kadoh at Chulalongkorn University for many helpful discussions. I am grateful to all members of the Theoretical Particle Physics group in Hiroshima university, particular Prof. Masanori Okawa and Dr. Issaku Kanamori. Additionally, thanks to the other peoples who help my smooth research. Finally, I would like to express my sincere appreciation for my friends and beloved family.

This numerical calculations in this work was supported by the Ministry of Education, Culture, Sports, Science and Technology (MEXT) as "Exploratory Challenge on Post-K computer" (Frontiers of Basic Science: Challenging the Limits), the Grant-in-Aid for JSPS Research Fellow (No.18J10663), JSPS KAKENHI Grant Numbers JP16K05328, JP19K03853 and the CUniverse research promotion project of Chulalongkorn Univesity (Grant CUAASC).

Appendix

A Generator of SU(3) group

Generators of SU(3) group is written by using Gell-Mann matrices λ_a ($a = 1, \ldots, 8$) as

$$T_a = \frac{\mathrm{i}}{2}\lambda_a. \tag{A.1}$$

Specific expressions of Gell-Mann matrices are as follows,

$$\lambda_0 = \begin{pmatrix} 1 & 0 & 0 \\ 0 & 1 & 0 \\ 0 & 0 & 1 \end{pmatrix}, \quad \lambda_1 = \begin{pmatrix} 0 & 1 & 0 \\ 1 & 0 & 0 \\ 0 & 0 & 0 \end{pmatrix}, \quad \lambda_2 = \begin{pmatrix} 0 & -\mathrm{i} & 0 \\ \mathrm{i} & 0 & 0 \\ 0 & 0 & 0 \end{pmatrix},$$
$$\lambda_3 = \begin{pmatrix} 1 & 0 & 0 \\ 0 & -1 & 0 \\ 0 & 0 & 0 \end{pmatrix}, \quad \lambda_4 = \begin{pmatrix} 0 & 0 & 1 \\ 0 & 0 & 0 \\ 1 & 0 & 0 \end{pmatrix}, \quad \lambda_5 = \begin{pmatrix} 0 & 0 & -\mathrm{i} \\ 0 & 0 & 0 \\ \mathrm{i} & 0 & 0 \end{pmatrix},$$
$$\lambda_6 = \begin{pmatrix} 0 & 0 & 0 \\ 0 & 0 & 1 \\ 0 & 1 & 0 \end{pmatrix}, \quad \lambda_7 = \begin{pmatrix} 0 & 0 & 0 \\ 0 & 0 & -\mathrm{i} \\ 0 & \mathrm{i} & 0 \end{pmatrix}, \quad \lambda_8 = \frac{1}{\sqrt{3}} \begin{pmatrix} 1 & 0 & 0 \\ 0 & 1 & 0 \\ 0 & 0 & -2 \end{pmatrix}. \tag{A.2}$$

T_a is anti-hermitian due to the property of Gell-Mann matrices, and it satisfy a orthonormality,

$$\mathrm{Tr}[T_a T_b] = -\frac{1}{2}\delta_{ab}, \tag{A.3}$$

and a commutation relation,

$$[T_a, T_b] = f_{abc} T_c. \tag{A.4}$$

f_{abc} is structure constants in SU(3) group which is completely antisymmetric for (a, b, c), and it satisfy

$$\begin{aligned} &f_{123} = 1, \\ &f_{147} = -f_{156} = f_{246} = f_{257} = f_{345} = -f_{367} = \frac{1}{2}, \\ &f_{456} = f_{678} = \frac{\sqrt{3}}{2}. \end{aligned} \tag{A.5}$$

Completeness of T_a is written as

$$T^a_{ij} T^a_{kl} = \frac{1}{2}\left(\delta_{il}\delta_{jk} - \frac{1}{N}\delta_{ij}\delta_{kl}\right), \tag{A.6}$$

and adjoint representations are given by

$$\mathrm{Ad}[T_a]_{bc} = -f_{abc}. \tag{A.7}$$

Bibliography

[1] K. G. Wilson, "Confinement of Quarks," Phys. Rev. D **10** (1974) 2445. doi:10.1103/PhysRevD.10.2445

[2] Z. Fodor and S. D. Katz, "A New method to study lattice QCD at finite temperature and chemical potential," Phys. Lett. B **534** (2002) 87 doi:10.1016/S0370-2693(02)01583-6 [hep-lat/0104001].

[3] C. R. Allton, S. Ejiri, S. J. Hands, O. Kaczmarek, F. Karsch, E. Laermann, C. Schmidt and L. Scorzato, "The QCD thermal phase transition in the presence of a small chemical potential," Phys. Rev. D **66** (2002) 074507 doi:10.1103/PhysRevD.66.074507 [hep-lat/0204010].

[4] S. Ejiri *et al.* [WHOT-QCD Collaboration], "Equation of State and Heavy-Quark Free Energy at Finite Temperature and Density in Two Flavor Lattice QCD with Wilson Quark Action," Phys. Rev. D **82** (2010) 014508 doi:10.1103/PhysRevD.82.014508 [arXiv:0909.2121 [hep-lat]].

[5] P. de Forcrand and O. Philipsen, "The QCD phase diagram for small densities from imaginary chemical potential," Nucl. Phys. B **642** (2002) 290 doi:10.1016/S0550-3213(02)00626-0 [hep-lat/0205016].

[6] P. de Forcrand and O. Philipsen, "The QCD phase diagram for three degenerate flavors and small baryon density," Nucl. Phys. B **673** (2003) 170 doi:10.1016/j.nuclphysb.2003.09.005 [hep-lat/0307020].

[7] M. D'Elia and M. P. Lombardo, "Finite density QCD via imaginary chemical potential," Phys. Rev. D **67** (2003) 014505 doi:10.1103/PhysRevD.67.014505 [hep-lat/0209146].

[8] L. K. Wu, X. Q. Luo and H. S. Chen, "Phase structure of lattice QCD with two flavors of Wilson quarks at finite temperature and chemical potential," Phys. Rev. D **76** (2007) 034505 doi:10.1103/PhysRevD.76.034505 [hep-lat/0611035].

[9] M. D'Elia and F. Sanfilippo, "The Order of the Roberge-Weiss end-point (finite size transition) in QCD," Phys. Rev. D **80** (2009) 111501 doi:10.1103/PhysRevD.80.111501 [arXiv:0909.0254 [hep-lat]].

[10] P. de Forcrand and O. Philipsen, "Constraining the QCD phase diagram by tricritical lines at imaginary chemical potential," Phys. Rev. Lett. **105** (2010) 152001 doi:10.1103/PhysRevLett.105.152001 [arXiv:1004.3144 [hep-lat]].

[11] K. Nagata, A. Nakamura, Y. Nakagawa, S. Motoki, T. Saito and M. Hamada, "Wilson fermions with imaginary chemical potential," PoS LAT **2009** (2009) 191 doi:10.22323/1.091.0191 [arXiv:0911.4164 [hep-lat]].

[12] K. Nagata and A. Nakamura, "Imaginary Chemical Potential Approach for the Pseudo-Critical Line in the QCD Phase Diagram with Clover-Improved Wilson Fermions," Phys. Rev. D **83** (2011) 114507 doi:10.1103/PhysRevD.83.114507 [arXiv:1104.2142 [hep-lat]].

[13] J. Takahashi, K. Nagata, T. Saito, A. Nakamura, T. Sasaki, H. Kouno and M. Yahiro, "Color screening potential at finite density in two-flavor lattice QCD with Wilson fermions," Phys. Rev. D **88** (2013) 114504 doi:10.1103/PhysRevD.88.114504 [arXiv:1308.2489 [hep-lat]].

[14] G. Aarts, "Can stochastic quantization evade the sign problem? The relativistic Bose gas at finite chemical potential," Phys. Rev. Lett. **102** (2009) 131601 doi:10.1103/PhysRevLett.102.131601 [arXiv:0810.2089 [hep-lat]].

[15] G. Aarts, L. Bongiovanni, E. Seiler, D. Sexty and I. O. Stamatescu, "Controlling complex Langevin dynamics at finite density," Eur. Phys. J. A **49** (2013) 89 doi:10.1140/epja/i2013-13089-4 [arXiv:1303.6425 [hep-lat]].

[16] D. Sexty, "Simulating full QCD at nonzero density using the complex Langevin equation," Phys. Lett. B **729** (2014) 108 doi:10.1016/j.physletb.2014.01.019 [arXiv:1307.7748 [hep-lat]].

[17] M. Cristoforetti *et al.* [AuroraScience Collaboration], "New approach to the sign problem in quantum field theories: High density QCD on a Lefschetz thimble," Phys. Rev. D **86** (2012) 074506 doi:10.1103/PhysRevD.86.074506 [arXiv:1205.3996 [hep-lat]].

[18] H. Fujii, D. Honda, M. Kato, Y. Kikukawa, S. Komatsu and T. Sano, "Hybrid Monte Carlo on Lefschetz thimbles - A study of the residual sign problem," JHEP **1310** (2013) 147 doi:10.1007/JHEP10(2013)147 [arXiv:1309.4371 [hep-lat]].

[19] M. Levin and C. P. Nave, "Tensor renormalization group approach to 2D classical lattice models," Phys. Rev. Lett. **99** (2007) no.12, 120601 doi:10.1103/PhysRevLett.99.120601 [cond-mat/0611687 [cond-mat.stat-mech]].

[20] Y. Shimizu, "Analysis of the $(1 + 1)$-dimensional lattice ϕ^4 model using the tensor renormalization group," Chin. J. Phys. **50** (2012) 749.

[21] Y. Shimizu and Y. Kuramashi, "Grassmann tensor renormalization group approach to one-flavor lattice Schwinger model," Phys. Rev. D **90** (2014) no.1, 014508 doi:10.1103/PhysRevD.90.014508 [arXiv:1403.0642 [hep-lat]].

[22] J. Unmuth-Yockey, Y. Meurice, J. Osborn and H. Zou, "Tensor renormalization group study of the 2d O(3) model," arXiv:1411.4213 [hep-lat].

[23] Y. Shimizu and Y. Kuramashi, "Critical behavior of the lattice Schwinger model with a topological term at $\theta = \pi$ using the Grassmann tensor renormalization group," Phys. Rev. D **90** (2014) no.7, 074503 doi:10.1103/PhysRevD.90.074503 [arXiv:1408.0897 [hep-lat]].

[24] S. Takeda and Y. Yoshimura, "Grassmann tensor renormalization group for the one-flavor lattice Gross?Neveu model with finite chemical potential," PTEP **2015** (2015) no.4, 043B01 doi:10.1093/ptep/ptv022 [arXiv:1412.7855 [hep-lat]].

[25] H. Kawauchi and S. Takeda, "Tensor renormalization group analysis of CP(N-1) model," Phys. Rev. D **93** (2016) no.11, 114503 doi:10.1103/PhysRevD.93.114503 [arXiv:1603.09455 [hep-lat]].

[26] Y. Meurice, A. Bazavov, S. W. Tsai, J. Unmuth-Yockey, L. P. Yang and J. Zhang, "Tensor RG calculations and quantum simulations near criticality," PoS LATTICE **2016** (2016) 325 doi:10.22323/1.256.0325 [arXiv:1611.08711 [hep-lat]].

[27] R. Sakai, S. Takeda and Y. Yoshimura, "Higher order tensor renormalization group for relativistic fermion systems," PTEP **2017** (2017) no.6, 063B07 doi:10.1093/ptep/ptx080 [arXiv:1705.07764 [hep-lat]].

[28] Y. Yoshimura, Y. Kuramashi, Y. Nakamura, S. Takeda and R. Sakai, "Calculation of fermionic Green functions with Grassmann higher-order tensor renormalization group," Phys. Rev. D **97** (2018) no.5, 054511 doi:10.1103/PhysRevD.97.054511 [arXiv:1711.08121 [hep-lat]].

[29] Y. Shimizu and Y. Kuramashi, "Berezinskii-Kosterlitz-Thouless transition in lattice Schwinger model with one flavor of Wilson fermion," Phys. Rev. D **97** (2018) no.3, 034502 doi:10.1103/PhysRevD.97.034502 [arXiv:1712.07808 [hep-lat]].

[30] Y. Kuramashi and Y. Yoshimura, "Three-dimensional finite temperature Z_2 gauge theory with tensor network scheme," arXiv:1808.08025 [hep-lat].

[31] D. Kadoh, Y. Kuramashi, Y. Nakamura, R. Sakai, S. Takeda and Y. Yoshimura, "Tensor network formulation for two-dimensional lattice $\mathcal{N} = 1$ Wess-Zumino model," JHEP **1803** (2018) 141 doi:10.1007/JHEP03(2018)141 [arXiv:1801.04183 [hep-lat]].

[32] D. Kadoh, Y. Kuramashi, Y. Nakamura, R. Sakai, S. Takeda and Y. Yoshimura, "Tensor network analysis of critical coupling in two dimensional ϕ^4 theory," arXiv:1811.12376 [hep-lat].

[33] Z.-C. Gu, X.-G. Wen "Tensor-entanglement-filtering renormalization approach and symmetry-protected topological order," Phys. Rev. B **80** (2009) 155131. doi:10.1103/PhysRevB.80.155131

[34] Z. Y. Xie, H. C. Jiang, Q. N. Chen, Z. Y. Weng and T. Xiang, Phys. Rev. Lett. **103** (2009) 160601 doi:10.1103/PhysRevLett.103.160601 [arXiv:0809.0182 [cond-mat.str-el]].

[35] G. Evenbly, G. Vidal "Tensor Network Renormalization," Phys. Rev. Lett. **115** (2015) 180405. doi:10.1103/PhysRevLett.115.180405

[36] R. P. Feynman, "Space-time approach to nonrelativistic quantum mechanics," Rev. Mod. Phys. **20** (1948) 367. doi:10.1103/RevModPhys.20.367

[37] K. G. Wilson, "Quarks and Strings on a Lattice," CLNS-321.

[38] K. Symanzik, "Continuum Limit and Improved Action in Lattice Theories. 1. Principles and phi**4 Theory," Nucl. Phys. B **226** (1983) 187. doi:10.1016/0550-3213(83)90468-6

[39] K. Symanzik, "Continuum Limit and Improved Action in Lattice Theories. 2. O(N) Nonlinear Sigma Model in Perturbation Theory," Nucl. Phys. B **226** (1983) 205. doi:10.1016/0550-3213(83)90469-8

[40] M. Luscher and P. Weisz, "On-Shell Improved Lattice Gauge Theories," Commun. Math. Phys. **97** (1985) 59 Erratum: [Commun. Math. Phys. **98** (1985) 433]. doi:10.1007/BF01206178

[41] B. Sheikholeslami and R. Wohlert, "Improved Continuum Limit Lattice Action for QCD with Wilson Fermions," Nucl. Phys. B **259** (1985) 572. doi:10.1016/0550-3213(85)90002-1

[42] M. Luscher, S. Sint, R. Sommer, P. Weisz and U. Wolff, "Nonperturbative O(a) improvement of lattice QCD," Nucl. Phys. B **491** (1997) 323 doi:10.1016/S0550-3213(97)00080-1 [hep-lat/9609035].

[43] L. Onsager, "Crystal statistics. 1. A Two-dimensional model with an order disorder transition," Phys. Rev. **65** (1944) 117. doi:10.1103/PhysRev.65.117

[44] B. Daufman, "Crystal Statistics. II. Partition Function Evaluated by Spinor Analysis," Phys. Rev. **76** (1949) 1232. doi:10.1103/PhysRev.76.1232

公表論文

(1) Irregular parameter dependence of numerical results in tensor renormalization group analysis.
Daisuke Kadoh, Yoshinobu Kuramashi, Ryoichiro Ueno,
·····Prog. Theor. Exp. Phys. 2019,
DOI:10.1093/ptep/ptz056

参考論文

(1) Numerical determination of the Λ-parameter in SU(3) gauge theory from the twisted gradient flow coupling,
Ken-Ichi Ishikawa, Issaku Kanamori, Yuko Murakami, Ayaka Nakamura, Masanori Okawa, Ryoichiro Ueno,
Published in PoS LATTICE2016 (2016) 185.

(2) Non-perturbative determination of the Λ-parameter in the pure SU(3) gauge theory from the twisted gradient flow coupling.
Ken-Ichi Ishikawa, Issaku Kanamori, Yuko Murakami, Ayaka Nakamura, Masanori Okawa, Ryoichiro Ueno,
Published in JHEP 1712 (2017) 067.